

DOT/FAA/TC-18/16

Federal Aviation Administration
William J. Hughes Technical Center
Aviation Research Division
Atlantic City International Airport
New Jersey 08405

Development of NexGen Burner Operations Setting for Fire Testing of Power Plant Components

October 2018

Final Report

This document is available to the U.S. public through the National Technical Information Services (NTIS), Springfield, Virginia 22161.

This document is also available from the Federal Aviation Administration William J. Hughes Technical Center at actlibrary.tc.faa.gov.



U.S. Department of Transportation
Federal Aviation Administration

NOTICE

This document is disseminated under the sponsorship of the U.S. Department of Transportation in the interest of information exchange. The U.S. Government assumes no liability for the contents or use thereof. The U.S. Government does not endorse products or manufacturers. Trade or manufacturers' names appear herein solely because they are considered essential to the objective of this report. The findings and conclusions in this report are those of the author(s) and do not necessarily represent the views of the funding agency. This document does not constitute FAA policy. Consult the FAA sponsoring organization listed on the Technical Documentation page as to its use.

This report is available at the Federal Aviation Administration William J. Hughes Technical Center's Full-Text Technical Reports page: actlibrary.tc.faa.gov in Adobe Acrobat portable document format (PDF).

Technical Report Documentation Page

1. Report No. DOT/FAA/TC-18/16		2. Government Accession No.		3. Recipient's Catalog No.	
4. Title and Subtitle DEVELOPMENT OF NEXGEN BURNER OPERATIONS SETTING FOR FIRE TESTING OF POWER PLANT COMPONENTS				5. Report Date October 2018	
				6. Performing Organization Code	
7. Author(s) Samir Tambe, Yi-Huan Kao, John Hasselbeck, and San-Mou Jeng				8. Performing Organization Report No.	
9. Performing Organization Name and Address Department of Aerospace Engineering and Engineering Mechanics University of Cincinnati Cincinnati, OH 45221-0070				10. Work Unit No. (TRAIS)	
				11. Contract or Grant No.	
12. Sponsoring Agency Name and Address U.S. Department of Transportation Federal Aviation Administration FAA National Headquarters 950 L'Enfant Plaza N SW 950 L'Enfant Plaza Washington, DC 20024				13. Type of Report and Period Covered Final Report	
				14. Sponsoring Agency Code AIR-6B3	
15. Supplementary Notes The FAA William J. Hughes Technical Center Aviation Research Division COR was Steven Summer.					
16. Abstract <p>The Next Generation (NexGen) (sonic) burner is a new burner designed by the FAA William J. Hughes Technical Center for the required FAA fire certification tests on power plant components. The objective of this study is to understand the performance of this burner and provide the benchmark to adapt the burner settings for future FAA fire tests. Tests have been conducted to study the burner performance and its sensitivity to operating conditions and changes in configuration. Tests were conducted on the old burner configuration consisting of the stator and turbulator, and the updated configuration consisting of the flame retention head and the static plate. Burner calibration was found to be sensitive to changes in fuel flow rate, but not to air mass flow rate, though burnthrough results were sensitive to both parameters. Results were not affected by fuel and air temperatures as long as the air mass flow rate was held constant at the different air temperatures. Changes in burner inclination were observed to affect the burner performance. For the updated burner configuration, tests were conducted to study the effect of changes in the internal configuration. The NexGen burner performance was observed to be robust, and tolerances have been specified for some of the internal configuration components.</p> <p>This report discusses ongoing developmental efforts related to the NexGen burner. It should be noted that the burner construction and settings discussed in this report are not representative of the most recent ones used on the NexGen burner. For detailed construction drawings and to view other documentation and presentations that discuss the most up-to-date burner configurations, please visit the FAA's Fire Safety Branch's website at www.fire.tc.faa.gov.</p>					
17. Key Words Fire tests, Power plant, Operation setting, Next generation burner			18. Distribution Statement This document is available to the U.S. public through the National Technical Information Service (NTIS), Springfield, Virginia 22161. This document is also available from the Federal Aviation Administration William J. Hughes Technical Center at actlibrary.tc.faa.gov .		
19. Security Classif. (of this report) Unclassified		20. Security Classif. (of this page) Unclassified		21. No. of Pages 72	22. Price

ACKNOWLEDGEMENTS

The authors wish to acknowledge support from the FAA William J. Hughes Technical Center. This work was conducted under grant No 10-G-003.

TABLE OF CONTENTS

	Page
EXECUTIVE SUMMARY	xi
1. INTRODUCTION	1
1.1 Introduction to Fire Tests	1
1.2 Fire Tests on Power Plant Components	1
1.3 Approved Burners for Power Plant fire tests	2
1.4 Burner Calibration Procedures	2
1.5 Temperature Measurement in a High-Temperature Environment	3
1.6 Objectives	3
2. NEXGEN BURNER	4
2.1 Background and Introduction	4
2.2 Original Configuration	4
2.3 Updated Configuration	7
3. EXPERIMENTAL SETUP	8
3.1 Burner Calibration	8
3.2 Fire Test	10
4. PREVIOUS WORK	12
4.1 Influence of Turbulator	12
4.2 Impact of TC Size	13
4.3 Burner Sensitivity to Operating Conditions	14
4.3.1 Sensitivity to Fuel Flow Rate	14
4.3.2 Sensitivity to Airflow Rate	14
4.3.3 Sensitivity to Total Flow Rate	16
4.4 Burner Sensitivity to test panel size	16
5. RESULTS AND DISCUSSION—OLD CONFIGURATION	17
5.1 Impact of Burner Orientation	17
5.1.1 Effect of Offset on Calibration	19
5.1.2 Burner Temperature and Heat-Flux Mapping	20
5.2 Effect of Fuel Temperature	22
5.3 Effect of Air Temperature	23

6.	RESULTS AND DISCUSSION—NEW CONFIGURATION	27
6.1	Influence of FRH and Fuel Nozzle: Fuel Spray	27
6.1.1	Flow Visualization	27
6.1.2	Fuel Flow Analysis	29
6.2	Influence of FRH and Fuel Nozzle: Burner Calibration mapping	31
6.3	Sensitivity of Burner to Operating Conditions	35
6.3.1	Baseline Test	35
6.3.2	Sensitivity to Fuel Flow Rate	36
6.3.3	Sensitivity to Fuel Temperature	37
6.3.4	Sensitivity to Air Mass Flow Rate	39
6.3.5	Sensitivity to Air Temperature	40
6.3.6	Baseline	42
6.3.7	Effect of Fuel-Nozzle Depth	43
6.3.8	Effect of Cone Depth	44
6.3.9	Effect of Cone Type	46
6.3.10	Effect of FRH deformation	48
7.	SUMMARY AND CONCLUSIONS	49
8.	REFERENCES	50

APPENDICES

A—TABLES FROM PREVIOUS WORK

B—DETAILED TABLES FOR CURRENT WORK

LIST OF FIGURES

Figure	Page
1 Schematic of Park DPL 3400 Burner	5
2 Schematic of the original configuration of the NexGen burner	5
3 Fuel and air-cooling mechanism for the NexGen burner	6
4 Modified turbulator	6
5 FRH mechanism: FRH, and static plate	7
6 FRH installation: partial, showing steel tube, and completed	7
7 Updated NexGen burner configuration	8
8 Temperature calibration setup	9
9 TCs used for temperature calibration, baseline 1/8 in. and smaller 1/16 in.	9
10 Heat Flux calibration setup	10
11 Setup for simultaneous temperature and heat-flux calibration	10
12 Typical test-panel installation	11
13 Comparison of exposed areas of different panel sizes relative to the NexGen burner	11
14 Back surface of Type A sample with exposed area and TC locations	12
15 Burner calibration using the original and modified turbulators	13
16 Comparison of burner damage for calibration using different TC sizes	14
17 Sensitivity of burner to fuel flow rate: average temperature and heat flux	14
18 Sensitivity of burner to airflow rate: average temperature and heat flux	15
19 Effect of airflow on burnthrough tests for type A panels, terminated at 17 min	15
20 Sensitivity of burner to total flow rate: average temperature and heat flux	16
21 Effect of airflow on burnthrough tests for type B panels, terminated at 10:00 min	16
22 Calibration locations: with 1 in offset, and no offset	18
23 Burnthrough times for different burner orientations	18
24 Effect of burner inclination on burnthrough tests for type B panels	19
25 Burner temperature maps (units °F) at different inclinations: 0°, 30°, 45°, and temperature mapping plane	21
26 Variation of average temperature with burner height at different burner orientations	21
27 Variation of heat flux with burner height at different burner orientations	22
28 Effect of fuel temperature on burner calibration: average temperature and heat flux	23
29 Effect of air temperature on burner calibration: average temperature and heat flux	24

30	Temperature trace of backside TC for tests T11–T14	25
31	Burnthrough times for different air temperature and pressure settings	26
32	Temperature trace of backside TC for tests T13–T16	27
33	FRHs	27
34	Spray visualization for different FRHs with the 2.25 GPH fuel nozzle: F3, F6, F12, F22, and F31	28
35	Spray visualization for different fuel nozzles for the F22 FRH: 2.0 GPH, 2.25 GPH, and 2.5 GPH	28
36	Spray distribution from optical patternator: measurement location, Delavan nozzle 1, Delavan nozzle 2, and Delavan nozzle 3	29
37	Pressure vs. flow for the three Delavan nozzles	30
38	Schematic of location of PDPA measurement	30
39	Flame shapes for different FRH and fuel nozzle sizes	32
40	Flame temperature maps (unit °F) for different FRH and fuel nozzles	33
41	Temperature calibration for different FRH and fuel nozzles	34
42	Heat flux profiles for different FRH and fuel nozzle	34
43	Temperature maps (unit °F) for baseline: Test T17 and Test T18	36
44	Heat flux profiles for the two baseline cases	36
45	Effect of fuel flow rate: temperature maps (unit °F): T19, less fuel, T18, baseline, and T20, more fuel	37
46	Effect of fuel flow rate: burnthrough	37
47	Effect of fuel temperature: temperature maps (unit °F): T21, $T_{\text{fuel}} = -1^{\circ}\text{C}$; T18 (baseline), $T_{\text{fuel}} = 6^{\circ}\text{C}$; T22, $T_{\text{fuel}} = 21^{\circ}\text{C}$; and T23, $T_{\text{fuel}} = 32^{\circ}\text{C}$	38
48	Effect of fuel temperature: burnthrough	38
49	Effect of airflow rate: temperature maps (unit °F): T24, less air, T18, baseline, and T25, more air	39
50	Effect of airflow rate: burnthrough	39
51	Effect of air temperature: temperature maps (unit °F): T26, $T_{\text{air}} = 4^{\circ}\text{C}$; T18 (baseline), $T_{\text{air}} = 10^{\circ}\text{C}$; T27, $T_{\text{air}} = 27^{\circ}\text{C}$; and T28, $T_{\text{air}} = 38^{\circ}\text{C}$	40
52	Effect of air temperature: burnthrough sensitivity of burner to configuration	41
53	Baseline temperature map, indicating region being tested	43
54	Baseline burnthrough times	43
55	Effect of fuel-nozzle depth: temperature maps (unit °F): -12.7 mm, baseline, +12.7 mm, map for -12.7 mm; map for baseline, and map for +12.7 mm	44
56	Effect of nozzle depth: burnthrough	44

57	Effect of cone depth: temperature maps (unit °F): cone moved back, baseline, cone moved forward, map for -50.8 mm, map for -25.4 mm, map for baseline, map for + 25.4 mm, and map for +50.8 mm	45
58	Effect of cone depth: burnthrough	46
59	Different cone types: baseline (stainless steel), ceramic insulated, Inconel, and FAA design (stainless steel)	46
60	Effect of cone type: temperature maps (unit °F): baseline (stainless steel) cone, ceramic-coated stainless steel cone, Inconel cone, and FAA design (stainless steel) cone	47
61	Effect of cone type: burnthrough	47
62	Deformation of FRH: baseline (undamaged), slightly deformed, and severely deformed	48
63	Effect of FRH deformation: temperature maps (unit °F): baseline (undamaged), slightly deformed, and severely deformed	48
64	Effect of FRH deformation: burnthrough	48

LIST OF TABLES

Table		Page
1	Test conditions for impact of burner orientation	17
2	Test conditions for impact of fuel temperature on calibration	23
3	Test conditions for impact of air temperature on calibration	24
4	Test conditions for impact of air temperature on burnthrough	25
5	Droplet size measurement for Delavan nozzles	31
6	Test conditions for influence of FRH and fuel nozzle	31
7	Test conditions for impact of burner operating conditions	35
8	Test conditions for impact of burner configuration	42

LIST OF ACRONYMS

AC	Advisory Circular
AWG	American Wire Gauge
CFR	Code of Federal Regulations
FRH	Flame retention head
ISO	International Standard
OD	Outer diameter
PDPA	Phase Doppler Particle Anemometry
RTD	Resistance temperature detector
SAE	Society of Automotive Engineers
SMD	Sauter mean diameter
TC	Thermocouple

EXECUTIVE SUMMARY

The Next Generation (NexGen, also known as Sonic) burner is a new burner developed at the FAA William J. Hughes Technical Center to replace out-of-production old kerosene burners used for conducting certification fire tests on aviation materials and components. The NexGen burner was initially developed for testing thermal/acoustic insulation and is being targeted for use in other fire tests, including power plant components. The configuration of the burner has also been revised, with the objective of improving burner performance and repeatability. The objective of this study is to provide the benchmark to adapt the burner settings for use in propulsion certification fire tests. The NexGen burner was found to satisfy the temperature and heat-flux requirements for power plant fire tests at certain operating conditions. The current study is an extension of a previous study with the same focus. The study detailed in the FAA report *Development of a Next-Generation Burner for Use in Testing Thermal Acoustic Insulation Burnthrough Resistance* (DOT/FAA/AR-TN09/23) focused on the original NexGen burner configuration with a modified turbulator. The turbulator was modified by adding four tabs, resulting in a more uniform flame, improving burner robustness. The effect of the size of thermocouples used in burner calibration was studied. The sensitivity of burner calibration and the results of burnthrough fire tests to changes in burner operating conditions were studied. Additionally, the effect of the size of test articles on burnthrough results was studied. The NexGen burner configuration was recently updated to replace the stator-turbulator with a Flame Retention Head (FRH). In the current study, additional tests were conducted on the old stator-turbulator configuration to assess the impact of burner inclination on calibration and burnthrough test results. Tests were also conducted on the updated NexGen burner configuration FRH to study the impact of burner operating conditions, orientation, and changes in burner configuration to burner performance. It was observed that changes in burner inclination affect burnthrough test results, so burner parameters need to be defined for each inclination level. Fuel and air mass flow rates and tolerances should be specified to ensure repeatability in fire test results. The NexGen burner has been shown to be robust as most changes in configuration were shown to not have any significant effects on burner performance. For the configuration changes that affect burner performances, tolerances have been recommended.

1. INTRODUCTION

1.1 INTRODUCTION TO FIRE TESTS

The FAA has established fire safety standards for various parts and components of aircraft. These standards are meant to ensure that material and components used in aircraft would survive a fire hazard for enough time to ensure survival of passengers and crew. Two different fireworthiness levels are defined: fire resistant and fireproof. These definitions are provided in Title 14 of the Code of Federal Regulations (14 CFR) Part 1 [1]. A material or component is said to be “fire resistant” if it can withstand the heat associated with fire at least as well as aluminum alloy; it is “fireproof” if it can withstand fire at least as well as steel [1]. Non-metallic components that inherently do not meet the Part 1 definition must be shown by test to provide equivalency to these requirements. Power plant components are required by the associated FAA regulations to meet fire resistant or fireproof standards, depending on their location on the aircraft and their function. The FAA has categorized material and components in an aircraft, and has prescribed guidelines and test procedures for each category. These can be found in the CFRs and in several Advisory Circulars (ACs). Materials or components that go in the engine or engine support are classified as power plant materials and are included in 14 CFR Parts 25 [2] and 33 [3], and are also covered by AC 20-135 [4]. An additional category is defined for fluid-carrying hoses used in the engine.

There are three ways to show a material or component complies with the fire resistant or fireproof requirements. The first method is to use material or a buildup of materials that meets the part 1 definition. Such components can be claimed to be fireproof by definition. The second way is to show a material or component provides equivalent performance by comparison to a previously approved component or a component that inherently meets the Part 1 definition. For example, the applicant may show by test and analysis that the construction and materials in a new component are equivalent to or superior to those in an older component, which was already certified as fireproof or fire resistant. In this case, the new component can be shown to be certifiable by comparison. In the case that either of the above methods is not applicable, compliance must be shown by test and analysis. The material or component can be certified by subjecting it to a fire test. In a fire test, the test article is exposed to a flame from a pre-approved burner, calibrated to certain standards. The calibration standards depend on the category of the test article. At the end of the fire test, if the test article meets the pass/fail criteria defined prior to the test, then the result can be used by the applicant to conduct an analysis of the installed configuration to show the results from the component test can be scaled up to show the installation meets the applicable CFR requirement.

1.2 FIRE TESTS ON POWER PLANT COMPONENTS

Power plant components that must meet fire protection standards are defined in the FAA regulatory standards. Examples of components that must meet fire protection standards include cowling, firewalls, flammable fluid tanks, flammable fluid carrying hoses, lines and components located in a fire zone, surfaces located within one nacelle diameter of the engine, fuel tank access panels and engine mounting systems. Regulatory documents for power plant components include FAA Engineering Report No 3A [5], AC 20-135 [4] and ISO 2685 [6]. AC 20-135 and ISO 2685 provide a test method and procedure for evaluating the compliance to the fire protection standards. Both AC 20-135 and ISO 2685 are equivalent, although there are a few differences between them. Some

of these differences, such as the flame calibration requirements (section 1.4) are discussed in following paragraphs. There are other standards available for these components from other regulatory organizations. An example is the Society of Automotive Engineers (SAE) regulations AS 1055, applicable for power plant hoses, which is equivalent to Power Plant Report 3A, although it has been updated recently.

AC20-135 and ISO 2685 provide more refined definitions for the categories fireproof and fire resistant, as applicable to power plant components. For power plant, “fire resistant” is the capability to withstand a standard flame (2000°F ± 150°F) for a 5-minute minimum, and “fireproof” is the capability to withstand the standard flame for a 15-minute minimum [4, 6].

The regulations for fire tests consist of requirements for burner calibration, test article setup, and operating conditions. The burner calibration procedure includes calibrating the burner flame temperature and the heat flux to specified values.

Because power plant components can vary significantly in size and application, it is not possible to define exact setup and test procedures for particular installation in the airplane. The applicant must assess the particular installation and develop a test plan that is approved by the certifying office prior to testing. However, several guidelines have been provided in the AC [4]. The components should be tested in their actual orientation, simulating the worst test conditions that the component may face on an aircraft. This could involve having fluid or airflow through the component at typical pressures. For power plant hoses, there is a recommended minimum flow based on the size of the hose, although the pressure in the hose should be the typical operating pressure. There is an additional requirement for vibration for all nonmetallic power plant components and for hoses. For components, the vibration requirement is an amplitude of 0.4 mm at the closest nonresonant frequency to 50 Hz, whereas for hoses the requirement is an amplitude of 1.6 mm at the closest nonresonant frequency to 33 Hz [6].

1.3 APPROVED BURNERS FOR POWER PLANT FIRE TESTS

The Power Plant Report 3A has a list of approved burners for use in power plant fire tests. The Power Plant Report 3A was published in 1978 and listed burners available at that time, including the Carlin 200 CRD, Stewart-Warner HPR 250, and the Stewart-Warner FR-600. However, these burners have been out of production for a long time. AC20-135 and ISO 2685 also refer to the Power Plant Report 3A for acceptable oil burners, and list the SAE AS401 gas burner as an acceptable burner. AC20-135 does have a provision for other burners being accepted, as long as they meet the fuel type, burner size requirement and the calibration requirement. The FAA Fire Test Handbook (<https://www.fire.tc.faa.gov/Handbook>), Chapter 11 lists the Park DPL 3400 burner in addition to the oil burners from Power Plant 3A, but this burner is also currently out of production.

1.4 BURNER CALIBRATION PROCEDURES

Two properties of the flame induced by the burner must be calibrated: flame temperature and heat flux. For burner calibrations, the regulations as listed in AC 20-135 [4] and ISO 2685 [6] are compared.

Flame-temperature calibration is conducted using Type-K, exposed bead, thermocouples (TC). ISO 2685 lists the use of a 7 TC rake, whereas AC 20-135 does not specify the number of TCs. There is also some variation on the specified TC size. AC 20-135 indicates an allowable size range of 1.59 mm (1/16 in.) to 3.18 mm (1/8 in.) sheath diameters, whereas ISO 2685 states that the TC sheath diameter should be ≤ 3 mm (0.12 in.).

Another difference in calibration requirements between the two documents involves the measured temperatures. ISO 2685 indicates that the temperature of each TC must be $1100 \pm 80^\circ\text{C}$ ($2012 \pm 144^\circ\text{F}$), whereas AC 20-135 defines the flame temperature for showing equivalency to steel or aluminum with a test flame of $1093 \pm 83^\circ\text{C}$ ($2000 \pm 150^\circ\text{F}$). AC 33.17-1A [7] clarifies the average temperature of the seven TCs should be equal to or higher than 1093°C (2000°F).

Two different methods of measuring the heat flux of the burner. The first method, specified in both AC 20-135 and ISO 2685, uses a heat-transfer device consisting of a 12.7 mm (0.5 in.) outer diameter (OD) copper tube with a constant 1 gal/min water flow rate through it. The amount of heat absorbed by the water, which is used to determine the burner heat flux, can be calculated from the temperature rise across the device. AC 20-135 also allows the use of a calorimeter, which can be used to measure the heat flux directly. There does exist a difference in the desired heat flux value between the two means of compliance guidelines. ISO 2685 requires heat flux to be in the range of $116 \pm 10 \text{ kW/m}^2$ ($10.2 \pm 0.9 \text{ BTU/ft}^2\text{-sec}$). AC 20-135 requires that the heat flux should be greater than 106 kW/m^2 ($9.3 \text{ BTU/ft}^2\text{-sec}$), and does not specify a maximum limit for the heat flux.

1.5 TEMPERATURE MEASUREMENT IN A HIGH-TEMPERATURE ENVIRONMENT

For flame temperature calibration, both AC 20-135 and ISO 2685 require the use of exposed bead, Type-K TCs to measure the temperature. However, there exists an inevitable temperature error between the measured temperature and real temperature because of heat losses, especially via radiation. Detailed analysis conducted in an earlier study [8] shows that the error in measurement is proportional to the fourth power of the measured temperature and is, therefore, quite large at the desired flame temperature. The report also provided a method to estimate the temperature error.

1.6 OBJECTIVES

The aim of this work is to understand the performance of the most recent configuration of the new NexGen oil-fueled burner and to provide a benchmark to adapt the burner settings for use in power plant fire tests. The evolution of the burner and configuration differences are discussed in section 2. Several parametric tests have been conducted on the original and the updated configuration of the NexGen burner to evaluate the burner performance and its sensitivity to operating parameters and configuration. In previous work on this project, the effect of the TC size used for flame calibration and a comparison of the NexGen burner with the gas burner were considered. The study also reported sensitivity of the burner to changes in operating conditions. The current work continues the study of the baseline NexGen configuration by studying the impact of burner inclination and fuel and air temperature on burner performance. Tests were also conducted on the updated NexGen burner configuration, consisting of the flame retention head (FRH) and the static plate. The sensitivity of the updated burner configuration to operating conditions and changes in configuration were studied.

2. NEXGEN BURNER

2.1 BACKGROUND AND INTRODUCTION

In August 2003, the FAA issued a final rule on the flammability of thermal acoustic insulation [9], which required that the thermal acoustic insulation installed in the lower half of all passenger-carrying aircraft be resistant to fire penetration during a crash accident. The compliance date was set for September 2009. This rule was identified in 14 CFR 25.856(b) [2] and was based on the use of the Park DPL 3400 burner for the fire test. However, shortly after the issuance of the Final Rule, it was discovered that the Park burner was no longer being produced, so there was a need to develop a suitable burner to replace the Park burner.

The NexGen burner was initially developed as a replacement to the Park burner for testing thermal acoustic insulation. Some of the geometric parameters of the Park burner were retained; the source of airflow was changed to compressed air, using a pressure regulator and a sonic choke to regulate the airflow rate and using a pressurized fuel tank or pump to provide fuel flow rate. The NexGen burner was developed in 2009 by Robert Ochs, and the development and early test results using the burner are provided in FAA Report AR-TN-09-23 [9].

2.2 ORIGINAL CONFIGURATION

A schematic of the Park burner (see figure 1), which used a blower fan and a small fuel pump, is housed on the burner body itself to supply the air and fuel to the burner. Because the NexGen burner was designed to replace the Park burner, the original concept of the burner used some of the same building blocks as the Park burner, including the body of the burner and the burner exit. Thus, the NexGen burner retains the same draft tube and exit cone as the Park burner. The significant differences were in the air-delivery and fuel-delivery mechanisms. The air-supply mechanism was changed to using air from a compressed air source, like a compressor, with a pressure regulator and a sonic choke to control and meter the airflow rate. The fuel supply was also from a pressurized fuel source. A schematic of the NexGen burner configuration is provided in figure 2. Details of the design and construction of the NexGen burner are provided in AR-TN-09-23 [9] and are briefly described in this section.

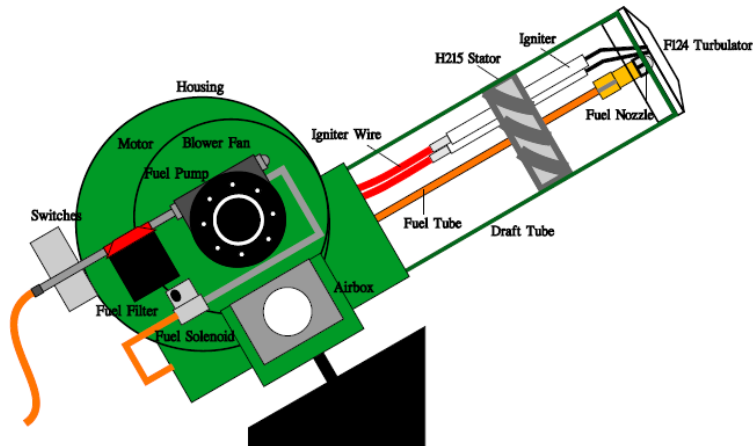


Figure 1. Schematic of Park DPL 3400 Burner

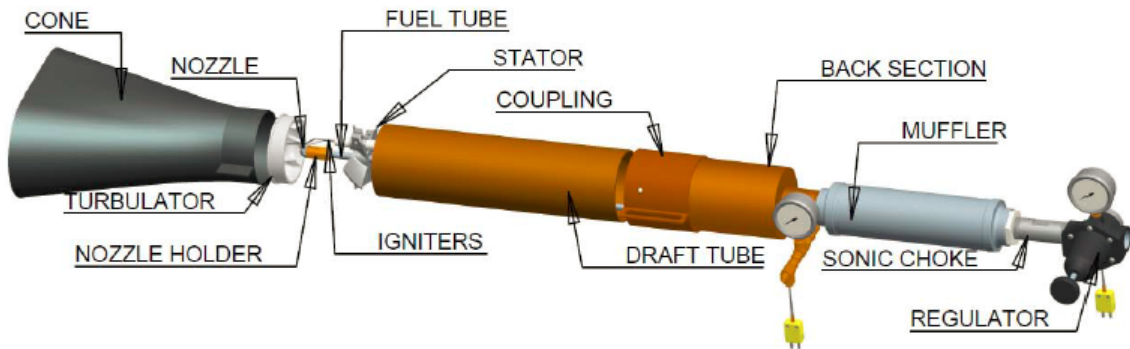


Figure 2. Schematic of the original configuration of the NexGen burner

The sonic choke was used to enable a precise method of controlling the airflow rate. The sonic choke features a convergent-divergent nozzle that is choked (i.e., has a shock wave) at the throat, so any disturbances upstream of the throat will not propagate into the burner body. The sonic choke also has a linear relationship between the pressure and the mass flow rate, so airflow rate can be controlled accurately using a precision air regulator. A muffer with a foam insert is used downstream of the sonic choke to reduce the noise from the choke and has been found to not have any significant effect on the burner performance.

The body of the burner consists of two sections of tubes connected by a coupler. The coupler is welded to the back section, whereas the forward section of the burner, called the draft tube, is held in the coupler by means of three set screws. The draft tube is identical to the one on the Park burner. The draft tube contains a Monarch H215 stator. The stator imparts swirl to the airflow. It also supports the fuel tube and the igniters. A Monarch F-124, 4 in x 2³/₄ in. turbulator is used at the end of the draft tube. The turbulator has internal vanes that provide a counter swirl to the swirl produced by the stator.

The fuel system for the NexGen burner has been changed to a pressurized fuel delivery system. Fuel is housed in a tank that is pressurized using a gaseous nitrogen bottle and a pressure regulator.

Fuel flow rate is monitored via fuel pressure by a pressure transducer. The fuel enters the burner via the fuel tube (see figure 2), which enters the back of the burner and runs along the center of the burner through the stator. The end of the burner tube has a fitting to accommodate the fuel nozzle. For the thermal acoustic insulation tests, the fuel nozzle used was a Monarch 5.5 GPH 80° PL nozzle [9]. For power plant and seat cushion tests, the nozzle was changed to a Monarch 2.25 80° PLP nozzle [10]. Ignition was achieved via electrodes mounted on the stator. A high-voltage transformer was used to create an arc between the electrodes.

The air and fuel inlet temperature to the burner was specified, with tolerances, to ensure burner repeatability between different test facilities. Cooling mechanisms were designed to meet cold air and fuel temperatures. Figure 3 shows a schematic of the cooling mechanism.

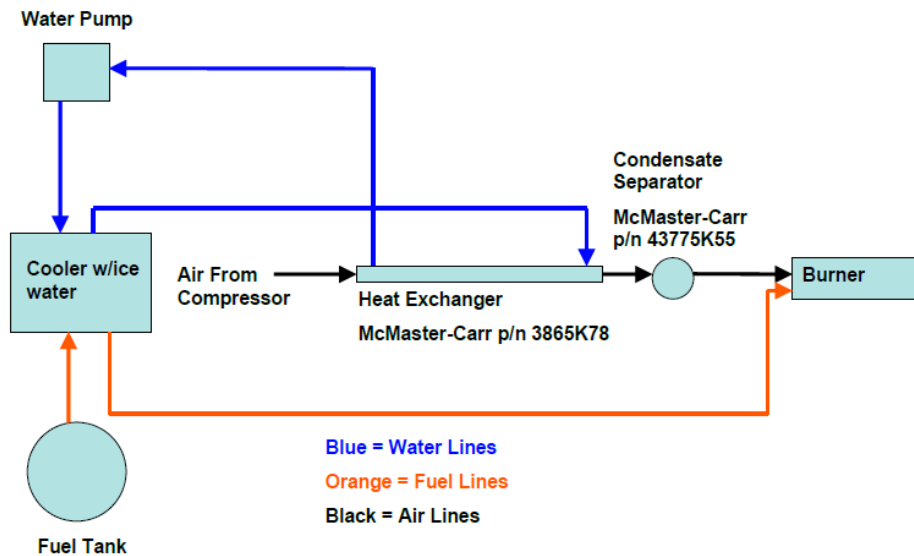


Figure 3. Fuel and air-cooling mechanism for the NexGen burner

For the burner used at University of Cincinnati, a few changes were made in the configuration. The turbulator was modified by adding four tabs at the 3, 6, 9, and 12 o'clock positions (see figure 4). These tabs are stainless steel and are 25.4 mm (1 in.) long, 19.1-mm (3/4 in.) wide, and 1.6 mm (1/16 in.) thick. Fuel supply was provided through a pump rather than from a pressurized tank. Ambient fuel and air were also used for some of the earlier tests. The cooling mechanism was employed for some of the later tests.



Figure 4. Modified turbulator

2.3 UPDATED CONFIGURATION

Because the NexGen burner is still being developed, a couple of changes were made to the burner configuration to improve the burner reliability and repeatability. The first change was made in the choice of fuel nozzles. The Monarch nozzles used in the original configuration were observed to have a deviation in flow rates of more than 13% [11]. An alternative nozzle, made by Delavan, was recommended for the burner used for seat-cushion tests [11]. These fuel nozzles were observed to have significantly less variability among different units. This fuel nozzle was later introduced for use on the burner for power plant fire tests in 2013 [12]. The nozzle selected for the power plant test was a Delavan W 2.25 GPH nozzle.

The second change was made in the airflow mechanism inside the burner tube. The old configuration featured a stator and turbulator to introduce counter-swirl into the airflow to stabilize the flame. In 2012, for the burner used for seat cushion tests, FRHs were introduced as possible alternatives to the stator-turbulator combination [13, 14]. The FRH was later incorporated into the burners used for the seat cushion [15] and power plant tests [12].

The FRH mechanism consists of two parts: a static plate and the FRH (see figure 5). The static plate forces the flow to the outside edge of the draft tube, whereas the FRH conditions the flow into an inner region and an outer region. The igniter electrodes and the fuel tube are mounted onto the static plate. The static plate and the FRH mount inside a steel tube, which fits inside the burner draft tube (see figure 6). Figure 7 shows a schematic of the completed new configuration. The FRH selected for the power plant test was the F31 FRH.

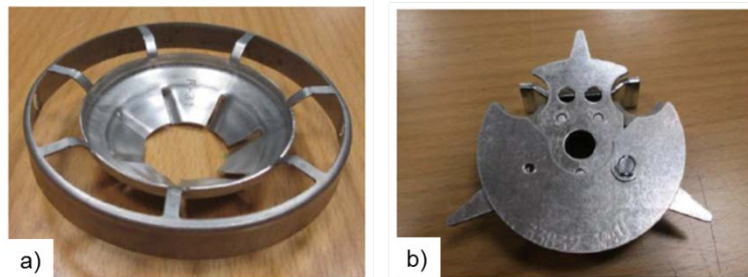


Figure 5. FRH mechanism: a) FRH, and b) static plate

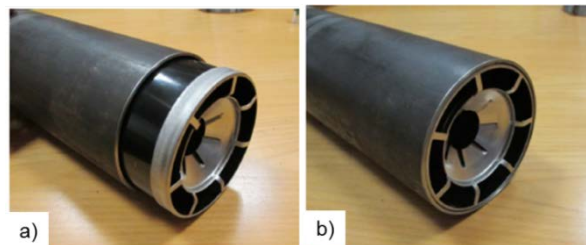


Figure 6. FRH installation: a) partial, showing steel tube, and b) completed

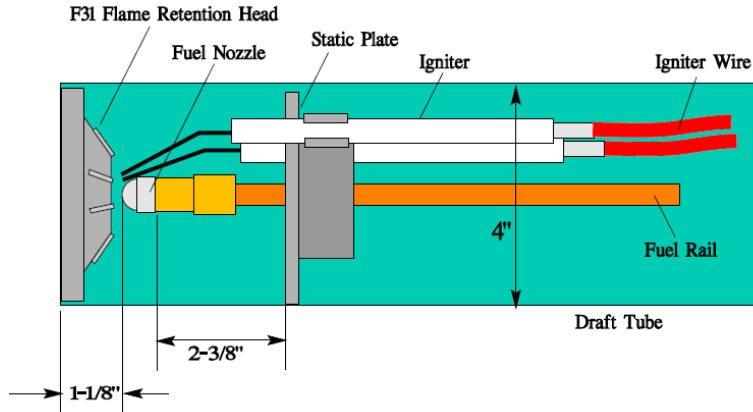


Figure 7. Updated NexGen burner configuration

3. EXPERIMENTAL SETUP

3.1 BURNER CALIBRATION

The process of burner calibration requires the measurement of the flame temperature and the heat-flux density of the burner. The flame temperature calibration is conducted using a rake of seven TCs. The TCs are arranged in a straight line, evenly spaced with a gap of 25.4 mm (1 in.) between them. The TC rake is installed so that the TC beads are located 101.6 mm (4 in.) from the exit plane of the burner and 25.4 mm (1 in.) above the burner centerline (see figure 8). The TCs used are type-K, exposed bead, with an SS sheath. The baseline TCs have a sheath diameter of 3.2 mm (1/8 in.) with a wire size of American Wire Gauge (AWG) 24 and a 0.5 mm (0.02 in.) diameter bead. To demonstrate the effect of TC size, a second type of TC was used, with a sheath diameter of 1.6 mm (1/16 in.). These TCs have a wire size of AWG 28 with a 0.3 mm (0.01 in.) diameter bead. Both sets of TCs are acceptable for burner calibration under AC20-135 [4], which lists an acceptable range of AWG 22–30 for wire sizes and 1/16–1/8 in. for the sheath sizes. Figure 9 shows the two kinds of TCs used.

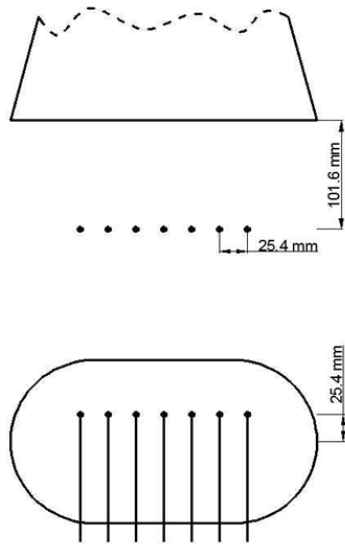


Figure 8. Temperature calibration setup [8]

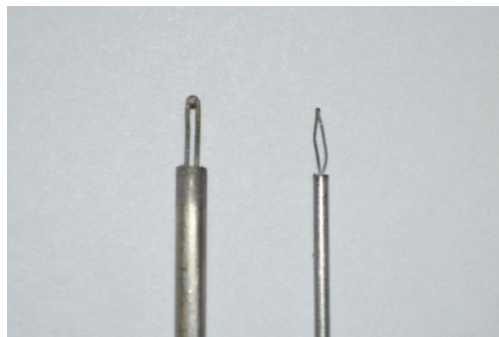


Figure 9. TCs used for temperature calibration, baseline 1/8 in. (left) and smaller 1/16 in. (right) [8]

Heat flux is measured by a heat-transfer device, which consists of a 12.7 mm (0.5 in.) OD copper tube with water flowing through it. The heat-transfer device is based on the concept originally provided in FAA Power Plant Engineering Report No. 3A [5], with some modifications. The significant modifications are the use of resistance temperature detectors (RTDs) instead of thermometers for the water temperature measurement, and the use of a ceramic insulation material instead of the asbestos tubing to insulate the copper tube outside of the exposed area. The RTDs, used to measure the inlet and outlet water temperature, have a 3.2 mm (1/8 in.) SS sheath. The location for heat-flux measurement is supposed to be the same as the temperature calibration, so the copper tube should be located 101.6 mm (4 in.) from the exit plane of the burner and 25.4 mm (1 in.) above the burner centerline (see figure 10).

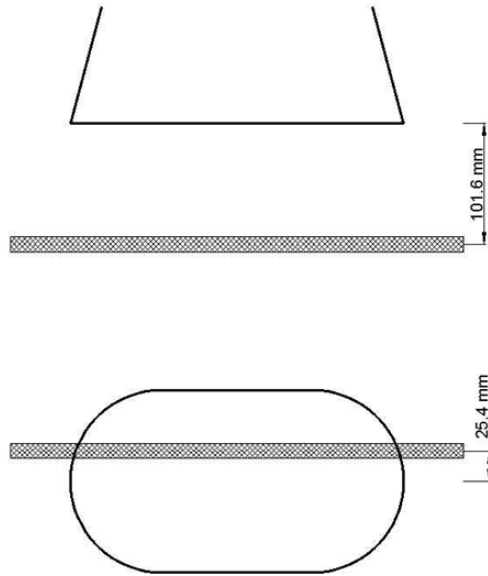


Figure 10. Heat Flux calibration setup [8]

The temperature and heat flux calibrations were conducted simultaneously for all the work presented here. The heat-transfer device was offset vertically and horizontally by approximately 6.4 mm (1/4 in.), so that the location was still within tolerance. Figure 11 shows a schematic of the setup for the simultaneous calibration.

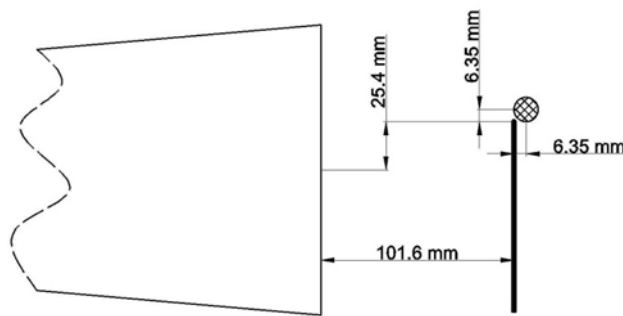


Figure 11. Setup for simultaneous temperature and heat-flux calibration [8]

3.2 FIRE TEST

Burnthrough fire tests were conducted on aluminum panels to compare burner performance. Three different panel sizes were used during of the project, labeled below as types A, B, and C. Types A and B were made from 6061 aluminum alloy and were 6.4 mm (1/4 in.) thick. Type A samples were 101.6 mm × 101.6 mm (4 in. × 4 in.), whereas Type B samples were 304.8 mm × 304.8 mm (12 in. × 12 in.) in size. Type C samples were made from 2024 aluminum alloy and were 3.2 mm (1/8 in.) thick with a size of 609.6 mm × 609.6 mm (24 in. × 24 in.). The test panels were installed by sandwiching them between a base plate and a sample holder plate, with ceramic gaskets used between the plates and the test panel to minimize heat transfer to the supporting plates. Figure 12

shows a schematic of a typical test panel installation. The base plate and the sample holder plate overlapped a portion of the test panels, so the exposed areas for panels A, B, and C were 76.2 mm \times 76.2 mm (3 in. \times 3 in.), 279.4 mm \times 279.4 mm (11 in. \times 11 in.), and 558.8 mm \times 558.8 mm (22 in. \times 22 in.), respectively. The test panels were installed so that the panel surface was 101.6 mm (4 in.) from the burner exit plane, and the center of the panel was at the same height as the burner centerline. Figure 13 shows the size and position of the different types of panels relative to the burner.

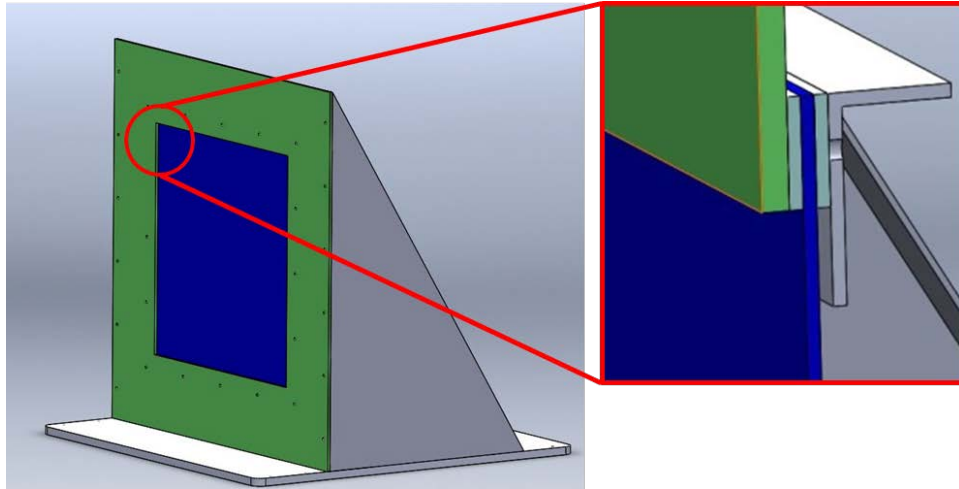


Figure 12. Typical test-panel installation

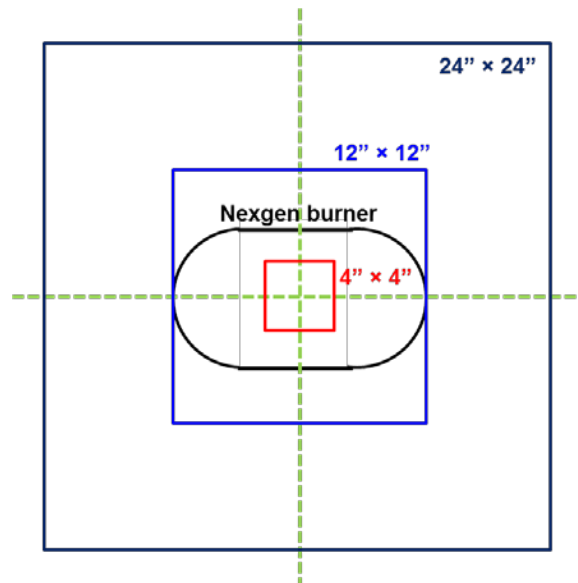


Figure 13. Comparison of exposed areas of different panel sizes relative to the NexGen burner

For panel types A and B, the test panels were instrumented with TCs on the back surface to monitor the surface temperatures. Three TCs were installed on each panel: one at the center and the other two located 25.4 mm (1 in.) away in the horizontal and vertical directions. The TCs used for surface

temperature were type K, ungrounded, with a 0.5 mm (0.020 in.) diameter SS sheath. The tips of the TCs were bonded to the panel surface using a high-temperature adhesive, Durabond™ 954. Figure 14 shows a schematic of a type A panel with the TC locations.

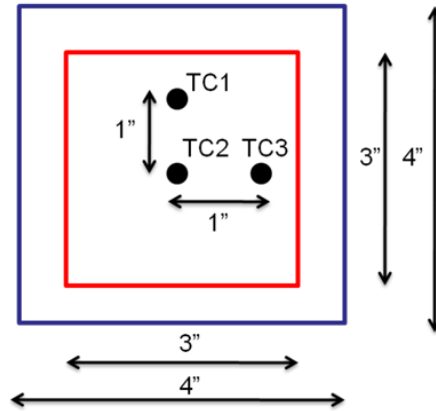


Figure 14. Back surface of Type A sample with exposed area and TC locations [8]

For panels type A and B, each test condition was repeated twice, with the first test usually carried out to burnthrough or terminated if the burnthrough did not occur after sufficient time. The second tests for each test condition were terminated at a predetermined time to allow comparison of damage caused by the burner after the same amount of flame exposure. The temperature traces from the TCs were used to confirm repeatability of test results. For panels of type C, which were not instrumented with TCs, each test condition was conducted twice, with both tests being carried out to burnthrough.

4. PREVIOUS WORK

Some of the research done in the project was published in a previous report, FAA report TC-13-38 [8]. This section presents a summary of those results.

4.1 INFLUENCE OF TURBULATOR

As listed in section 2.2, the turbulator was modified by adding tabs to it. It was observed that adding the tabs improved the fuel/air mixing, resulting in a shorter flame and a more uniform calibration temperature distribution (see figure 15). The test conditions are listed in the appendix A section in table A-1, which also lists the standard deviation of the seven TCs, which is lower for the modified turbulator. Moreover, with the modified turbulator, the burner was able to achieve the same average temperature with a slightly smaller fuel flow rate, which also produced lower heat flux. The modified turbulator has been used for all subsequent tests for the baseline NexGen configuration.

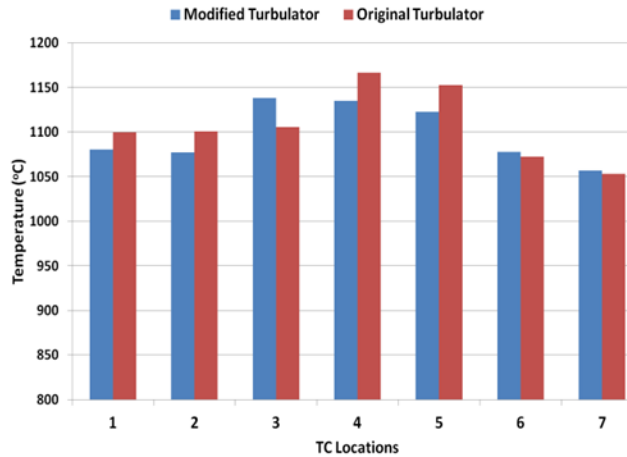


Figure 15. Burner calibration using the original and modified turbulators

4.2 IMPACT OF TC SIZE

As described in section 1.5 and in the previous work [8], the temperature measured by a TC is different from the temperature of the surrounding medium and depends on the medium temperature and the size of the TC bead. The error in measurement is proportional to the fourth power of the temperature and to the size of the TC bead.

Burner calibration and burnthrough tests were conducted on Type B samples using the baseline (3.2 mm) and the smaller (1.6 mm) TC sizes for temperature calibration. The burner parameters were adjusted to ensure satisfactory burner calibration for the tests. Test conditions for the calibration-only runs are listed in table A-2, whereas those for the burnthrough tests are listed as Tests #9, #10, #13, and #14 in table A-4 (see appendix A). From the calibration-only runs, it was observed that approximately 4% less fuel was required to achieve the same average calibration temperature using the smaller TCs, therefore also producing a smaller heat flux. This is similar to the findings of Ochs [16], who discovered that the smaller TCs measured an average of 100°F higher than the baseline TCs for the same burner-operating conditions.

For the burnthrough tests, tests #9 and #10 were conducted using the baseline TCs, whereas tests #13 and #14 used the smaller size TCs, with the first test of each set (#9 and #13) being conducted to burnthrough and the others terminated at 10 min for comparison of damage. For test #9, burnthrough occurred at 11.5 min, whereas test #13 was terminated at 15 min for lack of burnthrough. The panels for tests #10 and #14 (see figure 16) show some surface melting for test #10 and no damage for test #14. Therefore, it is clear from both the calibration and burnthrough data that the use of smaller TCs for calibration purposes result in a less severe fire test.

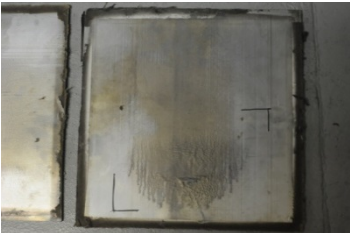
(a) Test #10, Calibrated by Baseline TCs (3.2 mm, 1/8 in.)	(b) Test #14, Calibrated by Smaller TCs (1.6 mm, 1/16 in.)
	
Surface melted	Undamaged

Figure 16. Comparison of burner damage for calibration using different TC sizes [8]

4.3 BURNER SENSITIVITY TO OPERATING CONDITIONS

4.3.1 Sensitivity to Fuel Flow Rate

Calibration trials with varying fuel flow rates at a constant airflow rate were conducted to study of the impact on burner performance. These trials are listed as cases #1 to #9 in table A-3 of appendix A. Figures 17(a) and (b) list the average temperature and heat flux for these calibration runs and clearly indicate increasing severity with a rise in the fuel flow rate.

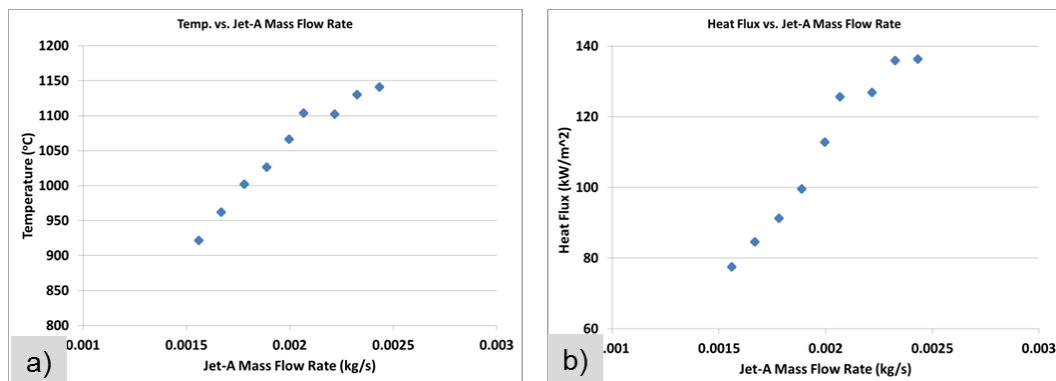


Figure 17. Sensitivity of burner to fuel flow rate: a) average temperature and b) heat flux [8]

4.3.2 Sensitivity to Airflow Rate

Calibration trials with varying airflow rates for a constant fuel flow rate were conducted to study the impact of airflow rates on burner performance. These trials are listed as cases #10 to #15 in table A-3 of appendix A. Figures 18(a) and (b) list the average temperature and heat flux for these calibration runs and do not show any significant effects from the change in airflow rate. It is well known that changes in airflow rates affect the equivalence ratio, so it is expected to affect the flame temperature. There is a possibility that temperature error and changes in the convective heat transfer may be responsible for the absence of variation in the burner calibration.

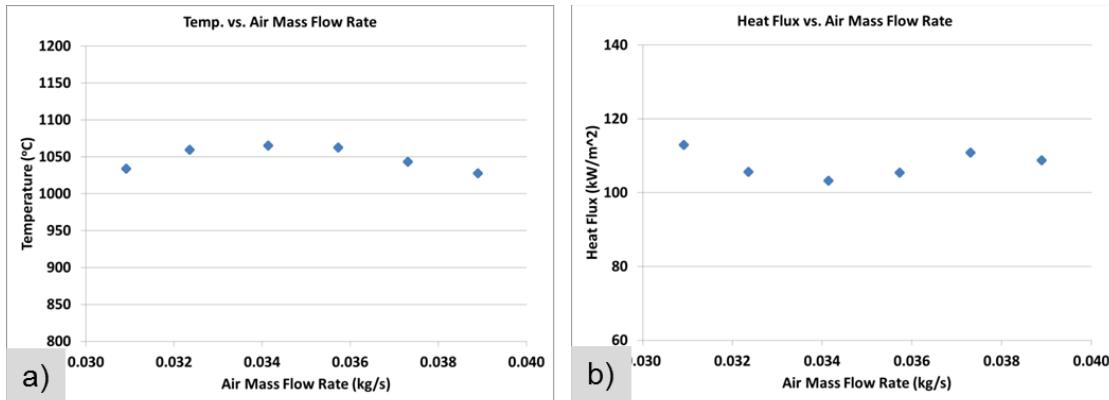


Figure 18. Sensitivity of burner to airflow rate: a) average temperature and b) heat flux [8]

To test this, burnthrough tests were conducted on Type A panels, reported as tests #1 to #6 in table A-4 in appendix A. Three cases were tested: a baseline (#3 and #4), a case with higher airflow (“leaner” equivalence ratio, #1, and #2), and a case with lower airflow (“richer” equivalence ratio, #5, and #6). Each test condition was conducted twice, with the first test run to burnthrough and the second terminated at 17 min. No burnthrough occurred for tests #1 to #4, and they were all terminated at 17 min. Figure 19 shows the test panels for tests #2, #4, and #6, respectively, showing that the damage to the test article increases progressively as the airflow decreases (equivalence ratio increases). Therefore, changes in airflow do affect the outcome of the fire test, even though this was not clearly observed in the calibration-only trials.

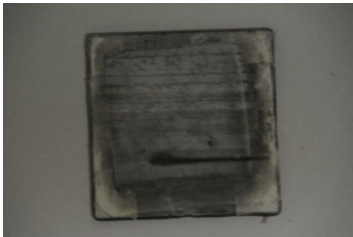
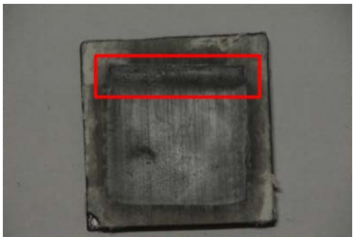
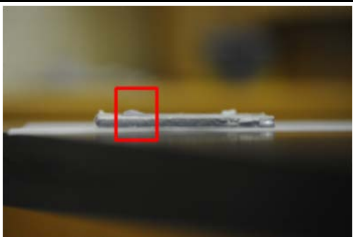
(a) Test #2, Fuel Leaner ($\Phi = 0.74$)	(b) Test #4, Baseline ($\Phi = 0.80$)	(c) Test #6, Fuel Richer ($\Phi = 0.87$)
		
		
Undamaged	Surface melted	Burned through

Figure 19. Effect of airflow on burnthrough tests for type A panels, terminated at 17 min [8]

4.3.3 Sensitivity to Total Flow Rate

Calibration trials with varying air and fuel flow rates were conducted while maintaining a constant equivalence ratio to study the impact of total flow rate on burner performance. Trials were conducted for four different equivalence ratios, and are listed as cases #16 to #41 in table A-3 of appendix A. Figures 20(a) and (b) list the average temperature and heat flux for these calibration runs, and clearly indicate increasing severity with an increase in the total flow rate. Increasing the total flow rate now involves an increase in the fuel flow rate as well, so the results are consistent with those seen in section 4.3.1.

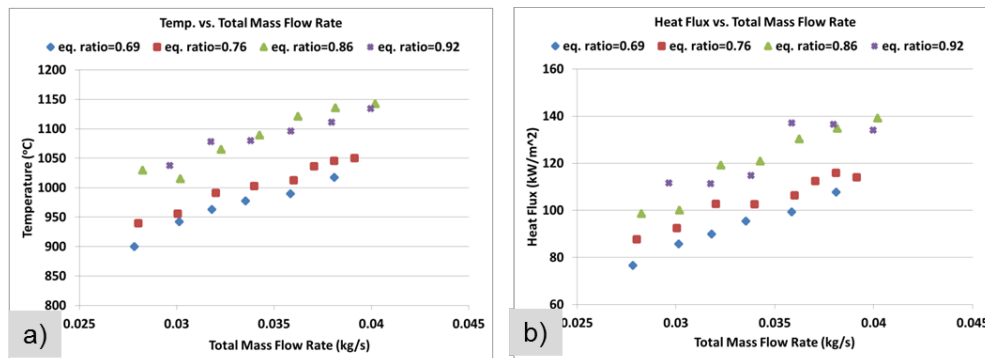


Figure 20. Sensitivity of burner to total flow rate: a) average temperature and b) heat flux [8]

4.4 BURNER SENSITIVITY TO TEST PANEL SIZE

To study the effect of panel size, the test conditions for tests #1 to #6 were repeated for the type B panels. These tests are reported as tests #6 to #12 in table A-4 of appendix A. Each test condition was conducted twice, with the first test run to burnthrough and the second terminated at 10 min. The effect of the change in the airflow was the same as for type A panels, with increasing severity as the airflow decreased (see figure 21), which shows the panels for which the tests were terminated at 10 min.

(a) Test #8, Fuel Leaner ($\Phi = 0.76$)	(b) Test #10, Baseline ($\Phi = 0.82$)	(c) Test #12, Fuel Richer ($\Phi = 0.88$)
		
Undamaged	Surface melted	Burned through

Figure 21. Effect of airflow on burnthrough tests for type B panels, terminated at 10:00 min [8]

Comparing the results for the two panel sizes, for the “richer” equivalence ratio, the type A panels burned through at 17 min, whereas the larger type B panels burned through much quicker, at 10 min. It is therefore evident that the size of the test article does have an impact on the outcome of the fire test, and emphasizes a need for uniform test article sizes to ensure consistent and repeatable results.

5. RESULTS AND DISCUSSION—OLD CONFIGURATION

5.1 IMPACT OF BURNER ORIENTATION

Fire tests were conducted to study the impact of the burner inclination to the calibration and results of burnthrough tests. Tests were conducted on Type B panels. Four different burner orientations were studied: 0° (i.e., horizontal [baseline]), 15°, 30°, and 45°. The test conditions and results are listed in table 1. The temperature calibration locations were still kept at 25.4 mm (1 in.) above the burner centerline, even for the inclined positions, as indicated in figure 22(a). The fuel flow rate was adjusted to get roughly the same average temperature for each burner orientation, the airflow rate being held constant. Each test condition was conducted twice, with the first test run to burnthrough and the second terminated at 10 min

Table 1. Test conditions for impact of burner orientation

Test Case	Orientation	Calibration offset	Jet-A	Air	Φ	Avg T	Heat Flux	Burnthrough Time	
			kg/s	kg/s		°C	kW/m ²	sec	
T1	0°	1 in.	1.92x10 ⁻³	3.78x10 ⁻²	0.76	1049	106.8	900	
T2						1049	106.8		
T3	15°		2.01x10 ⁻³	3.74x10 ⁻²	0.81	1050	117	640	
T4						1049	118.1		
T5	30°		2.17x10 ⁻³		0.87	1053	124.9	550	
T6						1054	126.1	570	
T7	45°		2.22x10 ⁻³		0.89	1054	129.5	600	
T8						1049	130.6	580	
T9	45°		No offset		2.15x10 ⁻³	0.86	1044	126.1	750
T10							1047	127.2	730

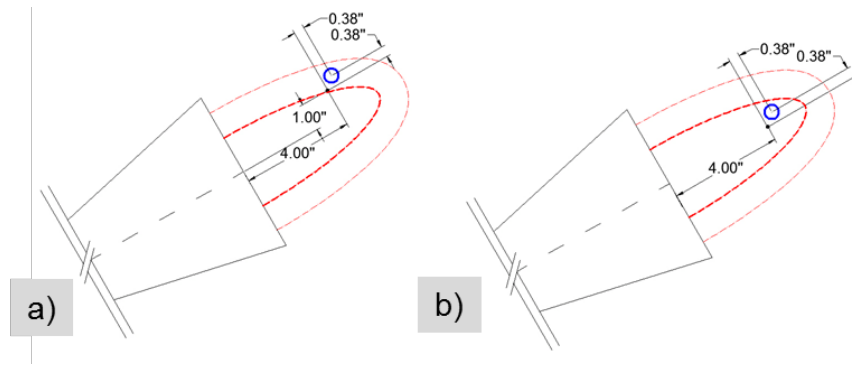


Figure 22. Calibration locations: a) with 1 in offset, and b) no offset

It was observed that the fuel flow rate needed to be increased with an increase in the inclination to obtain the same average calibration temperature, which was coupled with an increase in the heat flux, as seen from the calibration data in table 1. The burnthrough times (see figure 23) decrease with increasing burner inclination until an inclination of 30°; with a small increase in burnthrough time between 30° and 45°. This indicates that the burner severity increases with the inclination angle. Figure 24 shows the panels at the end of the second tests for each burner orientation (i.e., T2, T4, T6, and T8). It can be observed that there was no damage on the panel for the 0° orientation and only partial surface melting for the 15° orientation, whereas the panels for the 30° and 45° had already burned through at this stage.

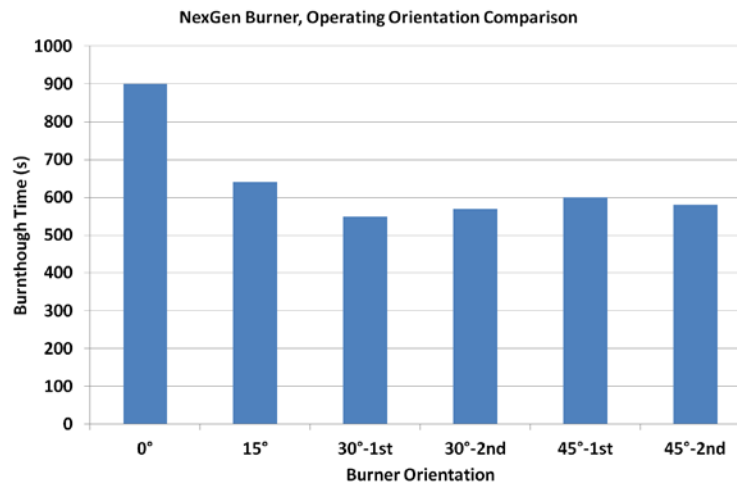


Figure 23. Burnthrough times for different burner orientations

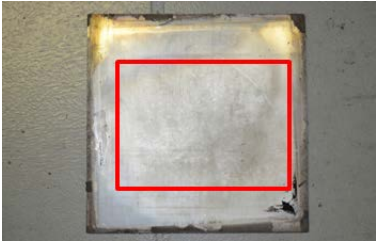
(a) T2, 0°, at 10:00	(b) T4, 15°, at 10:00
	
Undamaged	Surface damaged
(c) T6, 30°, at 9:30	(d) T8, 45°, at 9:40
	
Burnthrough	Burnthrough

Figure 24. Effect of burner inclination on burnthrough tests for type B panels

Therefore, changing the burner inclination did change the damage induced by the burner. From section 4.3.1, it might be conjectured that the increase in the burner severity could have been caused by the increase in the fuel flow rate. However, the fuel flow rate was increased to meet similar flame temperatures and, therefore, is due to the change in the burner inclination. This emphasizes the need to have burner parameters defined separately for different orientations.

5.1.1 Effect of Offset on Calibration

For the tests reported in section 4.2, the 25.4 mm offset between the TC rake and the burner centerline was maintained at all inclinations. For the standard burner orientation, which is horizontal, the vertical offset in the calibration location is applied to account for the buoyancy of the flame, which moves the location of the highest temperatures up above the burner centerline. However, because the burner is inclined, the effects of buoyancy are expected to decrease with the inclination angle. Therefore, the location of maximum temperature would probably not occur at the 25.4 mm offset location.

To study the effect of offset in the burner calibration location, the tests with the burner at 45° were repeated with the location of the burner calibration being moved to be aligned with the burner centerline, instead of the 25.4 mm offset. Figure 22 shows the change in the location of burner calibration, and tests T9 and T10 in table 1 list the test conditions for the no-offset case. It was observed that a lesser fuel-flow rate was required to get the same average temperature for the no-offset calibration, which also resulted in a lower heat flux. The burnthrough time of the panels increased from 10 min to slightly more than 12 min with the change in the calibration location. It should be noted that the case of 45° with no-offset calibration is still more severe than the baseline (0°) case.

Therefore, for different burner orientations, the buoyancy effect should be considered to prescribe the location of temperature calibration. Using the same calibration location for the horizontal burner ends up causing the burner to overcompensate to meet the same calibration requirements; therefore, the tests are more severe at higher inclinations.

5.1.2 Burner Temperature and Heat-Flux Mapping

Temperature and heat-flux maps of the NexGen burner at different orientations were obtained by traversing the calibration stand across the burner height. Temperature and heat-flux data were obtained at 12.7 mm (0.5 in.) increments along the burner vertical centerline. A rake of 11 TCs was used for this measurement to cover a total distance of 254 mm (10 in.) centered on the burner vertical centerline. The burner settings were fuel flow of 2.22×10^{-3} kg/s (2.6 GPH) and airflow at 3.78×10^{-2} kg/s (67.6 scfm). Figure 25 shows the temperature maps of the burner for inclinations of 0° , 30° , and 45° , respectively. Figure 25 also shows that the hot zone of the burner moves down, relative to the burner centerline, as the inclination angle increases. This supports the inference in section 5.1 and 5.1.1 that the effect of buoyancy becomes less pronounced as the burner inclination increases. Figure 26 shows the variation of the average flame temperature across the burner height for the different inclinations. This average temperature was obtained using the seven TCs in the center, making it equivalent to the average TC obtained from a regular calibration. Therefore, it can be seen that the height of the peak average temperature, relative to the burner centerline, decreases from 63.5 mm (2.5 in.) above at 0° to roughly 12.7 mm (0.5 in.) above for 45° . Figure 27 shows the variation of the heat flux with burner height for the different inclinations. It is observed that the locations of the maximum heat flux occur at almost the same heights as the average temperatures. The temperature and heat-flux maps underscore the necessity of prescribing specific calibration, and possibly test, guidelines to be used at different orientations.

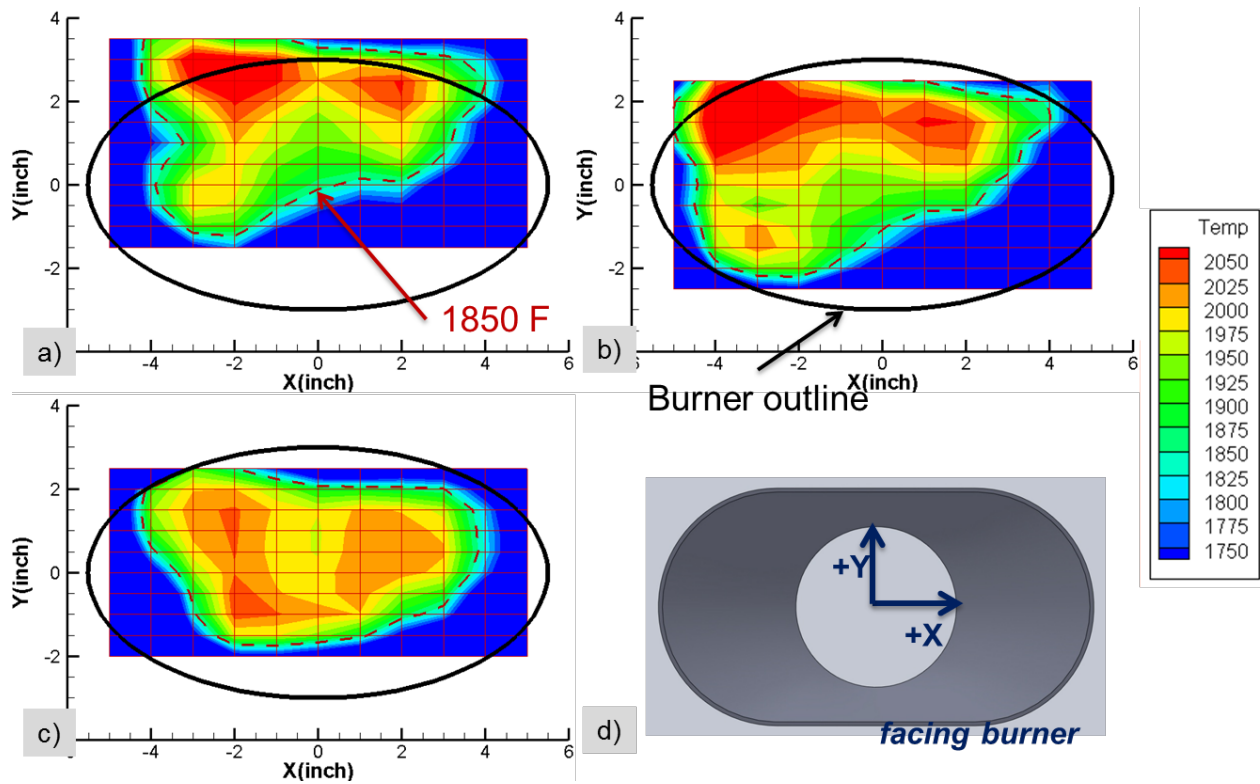


Figure 25. Burner temperature maps (units °F) at different inclinations: a) 0°, b) 30°, c) 45°, and d) temperature mapping plane

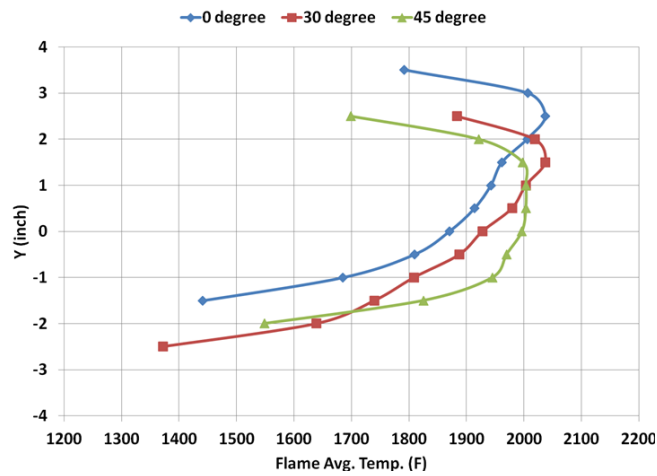


Figure 26. Variation of average temperature with burner height at different burner orientations

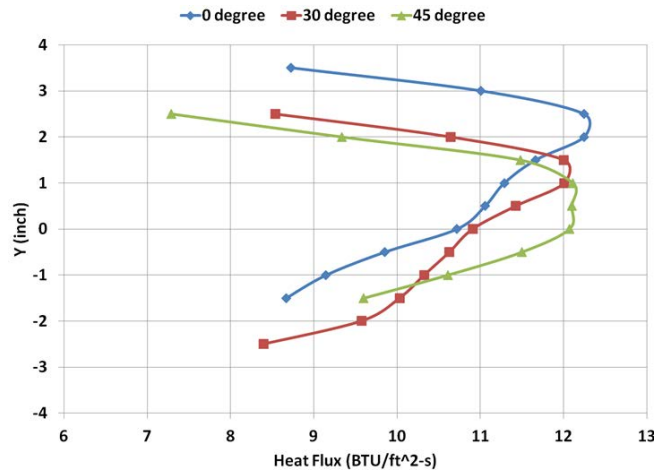


Figure 27. Variation of heat flux with burner height at different burner orientations

5.2 EFFECT OF FUEL TEMPERATURE

Calibration trials were conducted to study the effect of fuel temperature on burner calibration. Calibration trials were conducted for two different fuel-flow rates at four fuel temperature values, ranging from 15°C (59°F) to 52°C (125°F). These test conditions are listed in table 2. Figures 28(a) and (b) plot the trends of average temperature and heat flux with a change in the fuel temperature. It can therefore be seen that a change in fuel temperature did not have any significant effect on burner calibration.

Table 2. Test conditions for impact of fuel temperature on calibration

Test Case	Jet-A		Air	Φ	Avg T	Heat Flux
	kg/s	°C	kg/s		°C	kW/m ²
C1	2.14×10^{-3}	15	3.74×10^{-2}	0.84	1068	119.6
C2		33			1078	118.7
C3		39			1082	120
C4		52			1083	120.5
C5	2.37×10^{-3}	15		0.93	1118	130.4
C6		33			1122	134
C7		39			1131	134.7
C8		52			1132	130.8

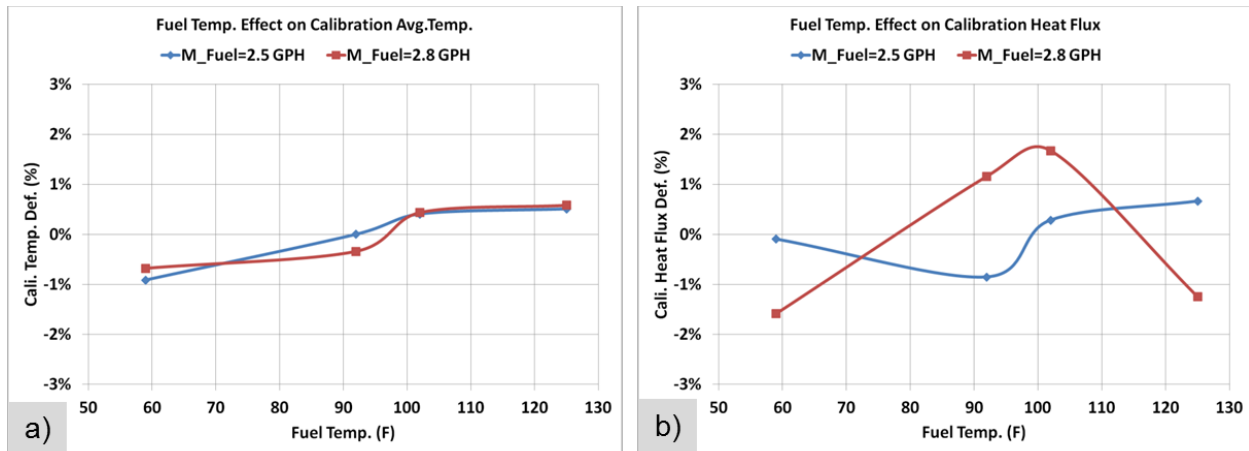


**Figure 28. Effect of fuel temperature on burner calibration:
a) average temperature and b) heat flux**

5.3 EFFECT OF AIR TEMPERATURE

Calibration trials were conducted to study the effect of air temperature on burner calibration. Calibration trials were conducted for two different fuel-flow rates at four air temperature values, ranging from 17°C (62°F) to 58°C (137°F). The air pressure setting was held constant. These test conditions are listed in table 3. Figures 29(a) and (b) plot the trends of average temperature and heat flux with a change in the fuel temperature. There is a trend of increase in the average temperature and heat flux with an increase in air temperature, although the changes are within tolerance of the mean values. Therefore, it can be seen that a change in air temperature did not have a significant effect on the burner calibration.

Table 3. Test conditions for impact of air temperature on calibration

Test Case	Fuel	Air			Φ	Avg T	Heat Flux kW/m ²
	kg/s	psig	kg/s	°C		°C	
C9	2.14x10 ⁻³	60	3.69x10 ⁻²	17	0.85	1048	117.5
C10			3.60x10 ⁻²	31	0.87	1056	118.6
C11			3.51x10 ⁻²	47	0.9	1062	118
C12			3.45x10 ⁻²	58	0.91	1073	120.7
C13	2.37x10 ⁻³		3.69x10 ⁻²	17	0.94	1104	129.8
C14			3.60x10 ⁻²	31	0.97	1111	133.2
C15			3.51x10 ⁻²	47	0.99	1119	132.2
C16			3.45x10 ⁻²	58	1.01	1126	135.4

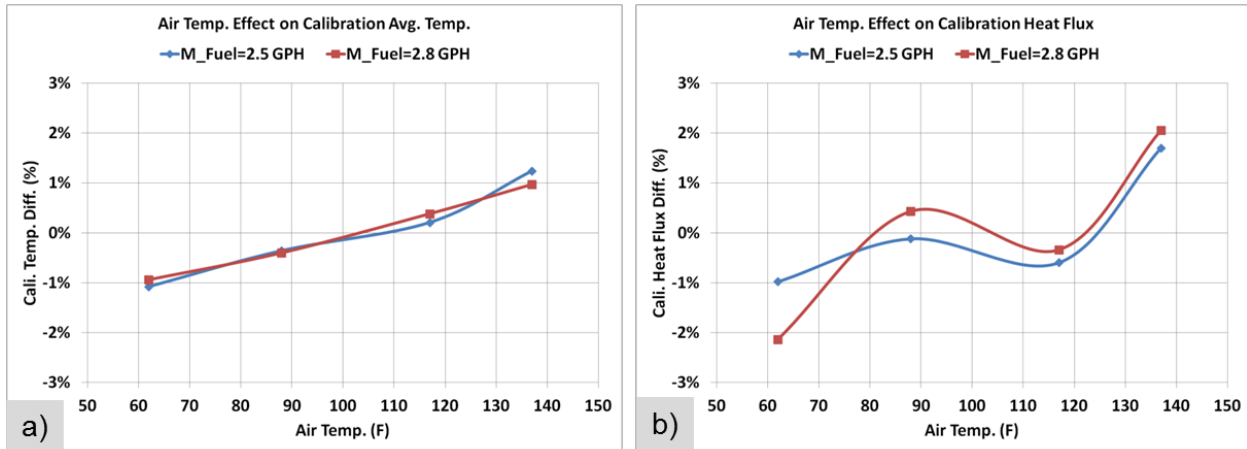


**Figure 29. Effect of air temperature on burner calibration:
a) average temperature and b) heat flux**

Burnthrough tests were conducted at two different air temperature settings, keeping the burner settings constant (constant air and fuel pressure). These tests are listed as tests T11–T14 in table 4.

Table 4. Test conditions for impact of air temperature on burnthrough

Test Case	Description	Fuel kg/s	Air			Φ	Avg T	Heat Flux	Burnthrough Time	
			psig	kg/s	°C		°C	kW/m ²	sec	
T11	cold @ 60 psi	2.23x10 ⁻³	60	3.62x10 ⁻²	28	0.91	1101	130.1	610	
T12				3.64x10 ⁻²	26	0.9	1098	129.1	600	
T13	hot @ 60 psi			3.46x10 ⁻²	57	0.95	1098	130.8	540	
T14				3.44x10 ⁻²	60	0.95	1105	131.5	510	
T15	cold @ 57 psi		2.23x10 ⁻³	57	3.48x10 ⁻²	27	0.94	1097	131.1	520
T16					3.49x10 ⁻²	25	0.94	1098	129.2	540

Tests were conducted on Type B panels instrumented with backside TCs. Figure 30 plots the backside temperatures for these tests, and the burnthrough times are shown in figure 31. The air temperature had a significant effect on the backside temperature and on burnthrough, with a faster temperature rise and quicker burnthrough being observed for the hot air case. There was no significant difference in the calibrations for the two cases.

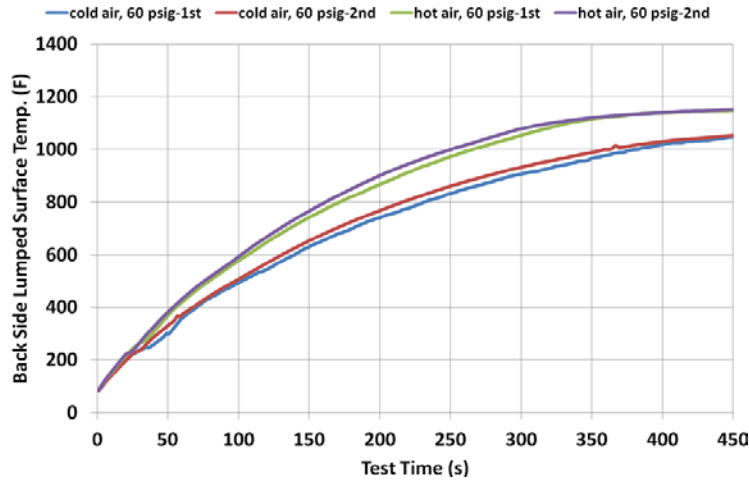


Figure 30. Temperature trace of backside TC for tests T11–T14

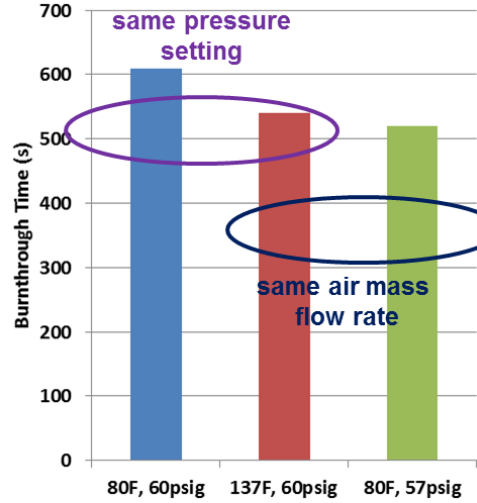


Figure 31. Burnthrough times for different air temperature and pressure settings

To understand the difference, we look at the impact of temperature on the airflow. The airflow through the burner is regulated by the pressure regulator and the sonic nozzle (i.e., it is a choked flow). The equation for mass flow through a sonic nozzle is:

$$\dot{m} = CA \sqrt{k\rho P \left(\frac{2}{k+1}\right)^{\frac{k+1}{k-1}}} \quad (1)$$

Thus,

$$\dot{m} \propto \sqrt{\rho P} \quad (2)$$

Now from ideal gas law,

$$\rho = \frac{P}{RT} \quad (3)$$

So,

$$\dot{m} \propto \frac{P}{\sqrt{T}} \quad (4)$$

Thus, for choked flow, the air mass flow decreases with an increase in temperature for the same pressure setting. Then, for the burnthrough tests, increasing the temperature essentially caused the equivalence ratio to increase, resulting in a fuel “richer” condition, similar to that seen in section 4.3.2 and causing earlier burnthrough.

To confirm this, additional tests were carried out at the ambient air temperature conditions, with the pressure setting adjusted to match the air mass flow rate of the heated air temperature condition. These tests are reported as tests T15–T16 in table 4. The resulting temperature plots are compared with that of the burnthrough times in figure 31 and the hot air case in figure 32. It can be observed

that as long as the air mass flow rate is maintained, the temperature rise and the burnthrough times remain unchanged, even with a change in the air temperature.

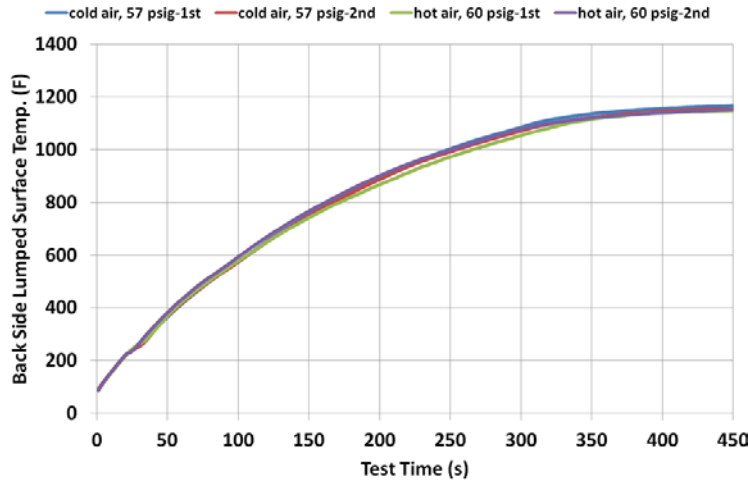


Figure 32. Temperature trace of backside TC for tests T13–T16

6. RESULTS AND DISCUSSION—NEW CONFIGURATION

6.1 INFLUENCE OF FRH AND FUEL NOZZLE: FUEL SPRAY

6.1.1 Flow Visualization

The effect of the different FRHs and the different fuel nozzle sizes on the fuel spray distribution was studied by spray visualization. Figure 33 shows the different FRHs used in this study. The spray was illuminated by a thin laser sheet, at the exit plane of the burner cone and was captured by a camera. The laser sheet and camera locations were maintained the same for all configurations to compare the different configurations.



Figure 33. FRHs

The test conditions for the spray visualization tests were a fuel flow rate of 1.92×10^{-3} kg/s (2.25 GPH) and airflow rate of 3.66×10^{-2} kg/s (65.3 scfm at 60 psi), with both fuel and air at ambient temperature. Figure 34 shows the fuel spray distribution for different FRHs for the baseline (2.25 GPH) fuel nozzle. Note that the spray was laterally symmetric; the images appear biased toward the side of the laser impingement. The fuel spray distribution is observed to become more uniform as the flow area of the FRH increases, which is equivalent to an increase in the FRH number.

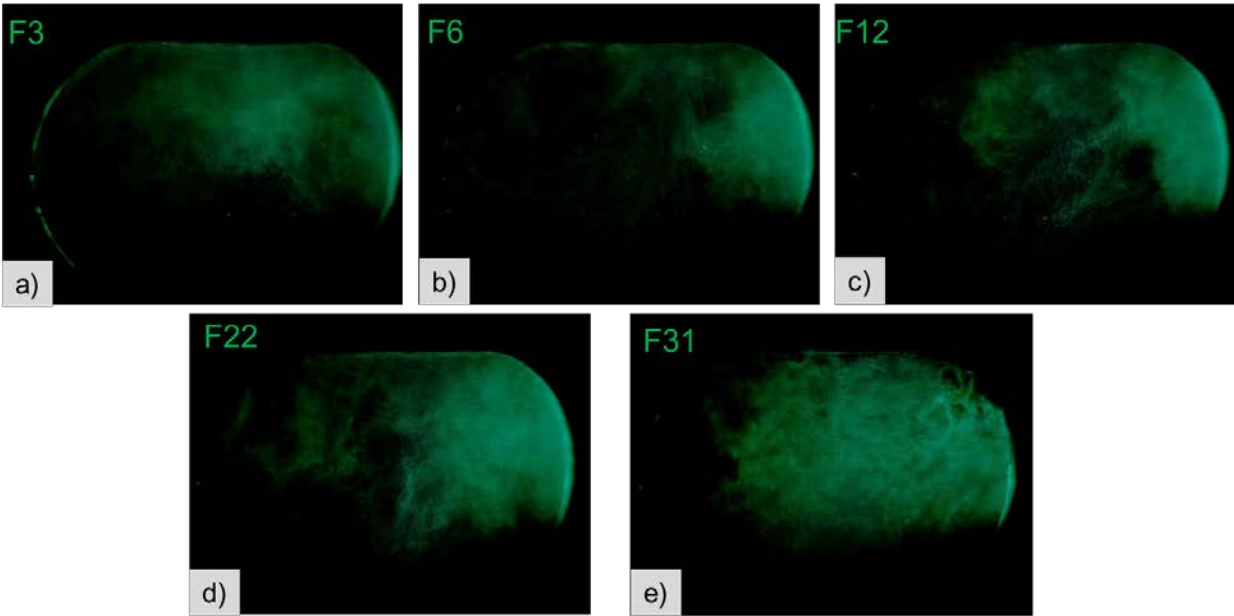


**Figure 34. Spray visualization for different FRHs with the 2.25 GPH fuel nozzle:
a) F3, b) F6, c) F12, d) F22, and e) F31**

Figure 35 shows the fuel spray distribution for the different flow number nozzles for the F22 FRH. It was observed that as the fuel nozzle flow number increases, the fuel spray becomes more uniform.

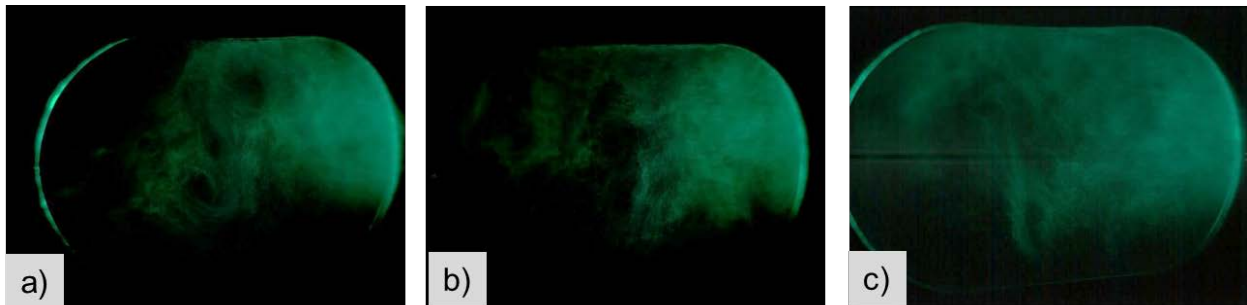


**Figure 35. Spray visualization for different fuel nozzles for the F22 FRH:
a) 2.0 GPH, b) 2.25 GPH, and c) 2.5 GPH**

6.1.2 Fuel Flow Analysis

A detailed analysis of the fuel spray from the fuel nozzles was conducted to study the repeatability between different fuel nozzle units of the same type. Three different units of type W, 2.5 GPH, fuel nozzles were used in this study. Optical patterning, flow number checks, and droplet sizing measurements were conducted for the three units.

Figure 36 shows the cross-section of the spray as measured using the optical patternator. Measurement was conducted 76.2 mm (3 in.) downstream of the injection location (see figure 36(a)). The spray patterns show a solid cone spray, with very high concentration in the center. The sprays from the different units looked similar, indicating a good reproducibility between different units of the same nozzle model.

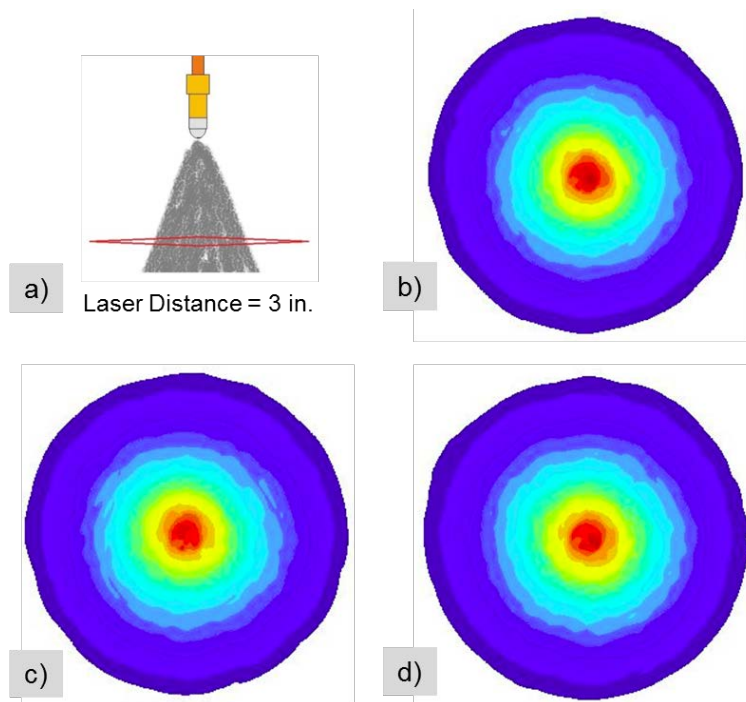


Figure 36. Spray distribution from optical patternator: a) measurement location, b) Delavan nozzle 1, c) Delavan nozzle 2, and d) Delavan nozzle 3

The fuel flow rates through the three units were varied to study the flow versus pressure behavior of the units. Figure 37 plots the flow rate versus the pressure for the nozzles. There was again a very good agreement between the three nozzles.

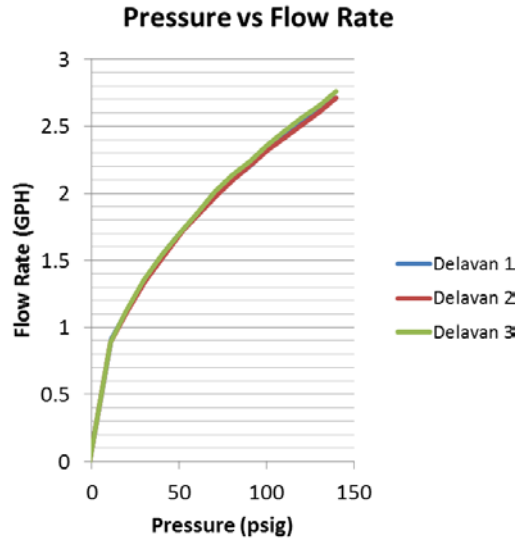


Figure 37. Pressure vs. flow for the three Delavan nozzles

Additionally, droplet size measurements were conducted for the three nozzle units. The droplet size measurement was carried out using Phase Doppler Particle Anemometry (PDPA). Because the PDPA conducts measurement only at 1 point at a time, the measurements were conducted along the centerline of the nozzle, 25.4 mm (1 in.) downstream of the nozzle tip (see figure 38). The values of the average diameter and the Sauter mean diameter (SMD) (see table 5) show very good comparison between the different units.

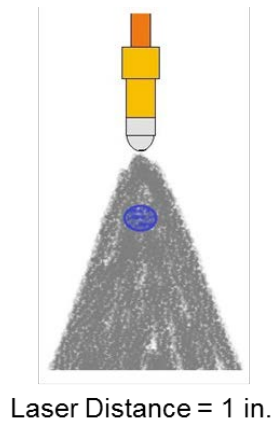


Figure 38. Schematic of location of PDPA measurement

Table 5. Droplet size measurement for Delavan nozzles

Nozzle	SMD
Delavan #1	12.7
Delavan #2	13.0
Delavan #3	13.2

The three nozzles tested for the same fuel nozzle line exhibited very good repeatability. Therefore, the Delavan fuel nozzles being used in the new configuration have been shown to be significantly more repeatable compared with the Monarch fuel nozzles being used for the old configuration.

6.2 INFLUENCE OF FRH AND FUEL NOZZLE: BURNER CALIBRATION MAPPING

Temperature and heat flux maps of the burner were carried out for the new burner using the different FRH and fuel-nozzle sizes. A nine-TC rake was used for the temperature maps to cover the area of ± 101.6 mm (4 in.) from the vertical centerline. Temperature and heat-flux measurements were carried out in vertical increments of 12.7 mm (0.5 in.). The F12, F22, and F31 FRHs as well as 2.0, 2.25, and 2.5 GPH nozzles were used in the study. Airflow rate was maintained at 3.66×10^{-2} kg/s (65.3 scfm at 60 psi, ambient) whereas fuel pressure was adjusted to obtain the design flow rate for all nozzles. The test conditions are listed in table 6.

Table 6. Test conditions for influence of FRH and fuel nozzle

Test Case	FRH	Fuel Nozzle	Fuel	Air	Φ	Avg T	Heat Flux
			kg/s	kg/s		$^{\circ}\text{C}$	kW/m^2
C17	F22	2.0	1.58×10^{-3}	3.64×10^{-2}	0.64	882	107.9
C18	F31	2.0				944	123.8
C19	F12	2.25	1.79×10^{-3}		0.72	956	140.8
C20	F22	2.25				969	136.3
C21	F31	2.25				1001	138.5
C22	F22	2.5	1.96×10^{-3}		0.79	1006	156.7
C23	F31	2.5				1022	159

Figure 39 shows pictures of the flame shapes for the different FRH and fuel nozzle sizes. For a given fuel nozzle, the flame spread increases with increased FRH flow area. This flow area is designated by the increase in FRH number. However, for a given FRH, the flame coverage increases with the fuel nozzle size (flow rate).

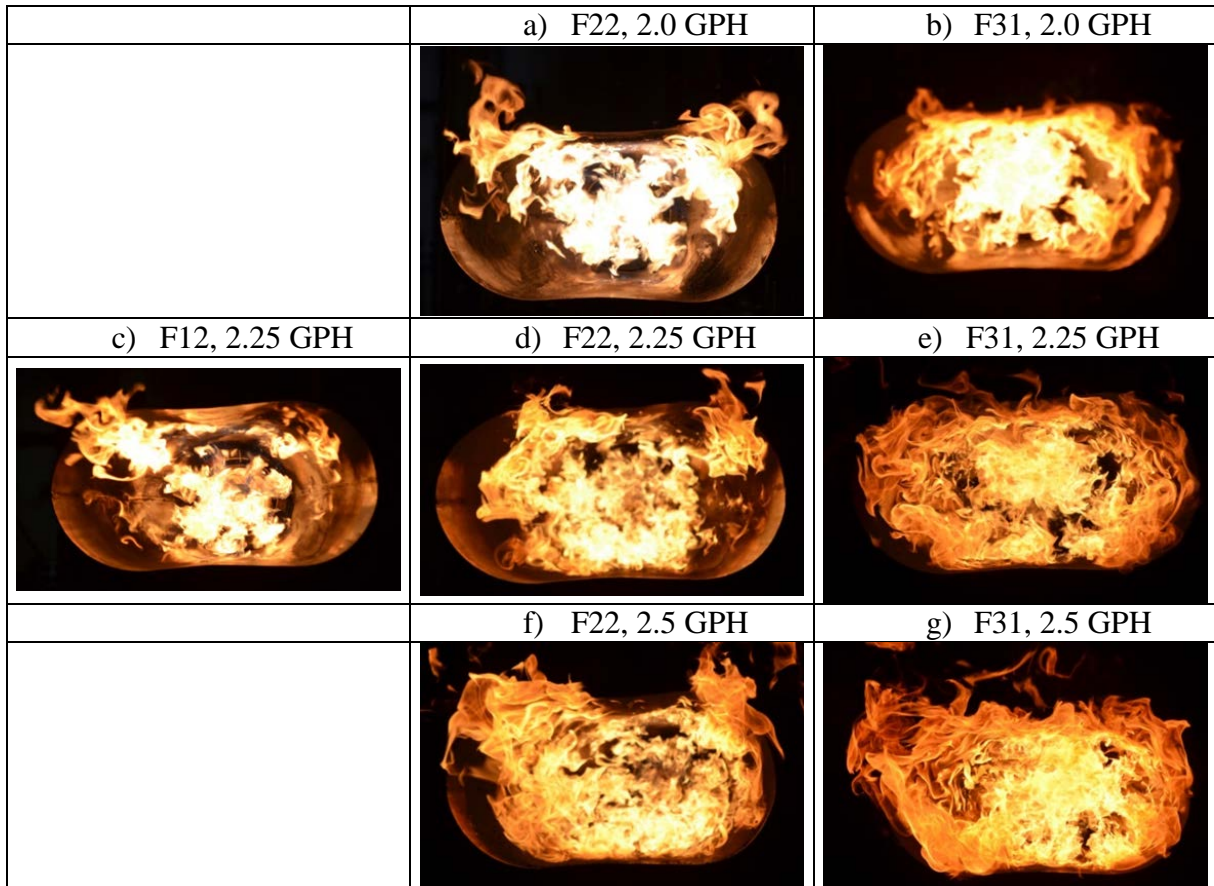


Figure 39. Flame shapes for different FRH and fuel nozzle sizes

Figure 40 shows the calibration temperature maps for the same cases as in figure 39. Similar to the observation of flame sizes, it was observed that the size of the hot zone increases with an increase in the FRH area and with an increase in the flow number of the fuel nozzle.

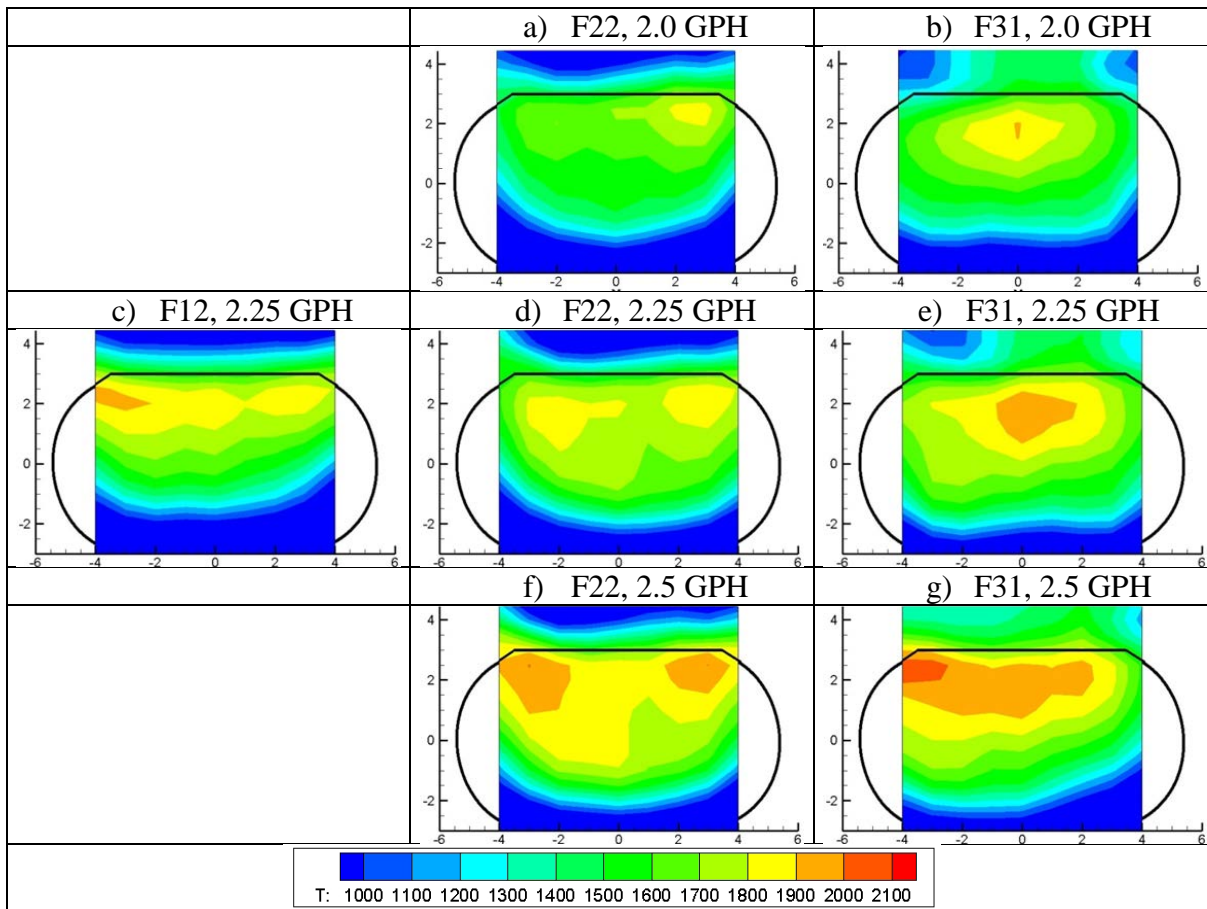


Figure 40. Flame temperature maps (unit °F) for different FRH and fuel nozzles

Figure 41 plots the temperature traces of the seven center TCs at the regular calibration location (25.4 mm above centerline) cases previously shown. This represents the typical burner temperature calibrations. From figure 41 and table 6, it can be observed that the temperature profiles for the F22 FRH were nearly flat, indicating more uniform fuel distribution. The temperature profiles for the F31 FRH were peaked at the center and exhibited the highest average temperature for all the FRHs for a given fuel nozzle. For all FRHs, increasing the fuel nozzle size increased the average flame temperature.

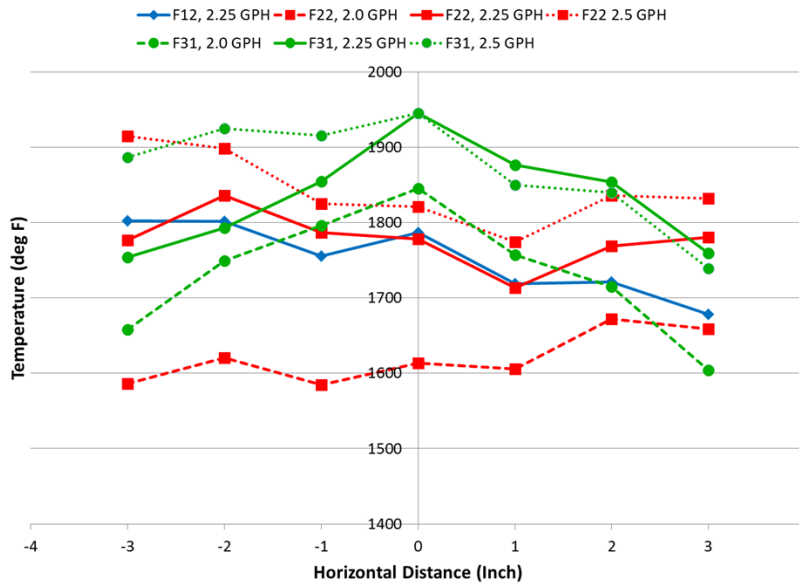


Figure 41. Temperature calibration for different FRH and fuel nozzles

Figure 42 shows the variation of heat flux across the height of the burner for the different cases studied. Each configuration has a peaked distribution at a location above the centerline, with the heat flux dropping above and below this location. For the F12 and F22 FRHs, the peak heat flux occurs at a height of 50.8 mm (2 in.) above the burner centerline, whereas for F31, the location of peak heat flux is 25.4 mm (1 in.) above the burner centerline. For the same fuel nozzle, the magnitude of the peak heat flux decreased as the FRH area increased, whereas for a given FRH, the magnitude of the peak heat flux increases with the fuel flow.

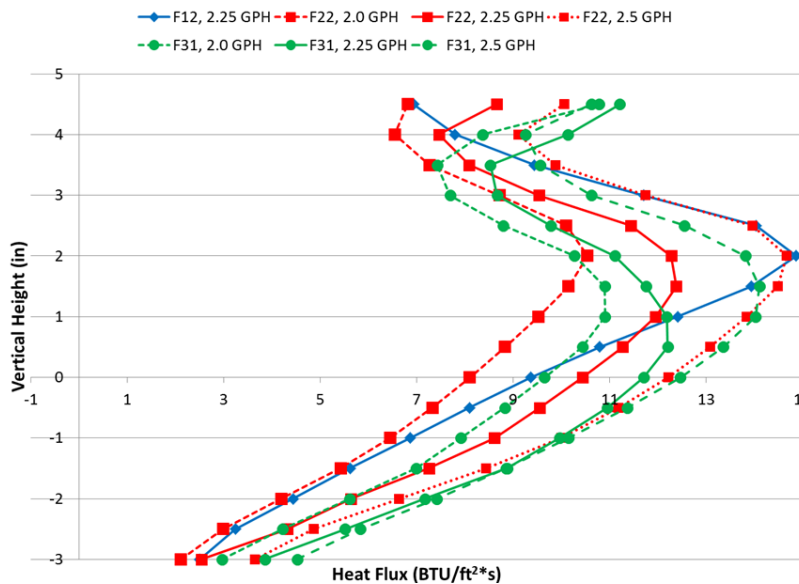


Figure 42. Heat flux profiles for different FRH and fuel nozzle

6.3 SENSITIVITY OF BURNER TO OPERATING CONDITIONS

Tests were conducted to study the sensitivity of the new NexGen burner configuration to changes in operating conditions. The new configuration consisted of the F31 FRH, and the 2.5 GPH type W fuel nozzle. The sensitivity of burner performance to fuel and airflow rates and temperature was studied. All tests consisted of temperature and heat flux mapping, conducted at vertical increments of 12.7 mm (0.5 in.). A rake of nine-TCs was used for the temperature mapping. At each test condition, burnthrough tests were conducted on type C panels. The test conditions for these tests are listed in table 7.

Table 7. Test conditions for impact of burner operating conditions

Test Case	Description	Fuel		Air			Φ	Avg T °C	Heat Flux kW/m ²	Burnthrough Time sec
		kg/s	°C	psig	kg/s	°C				
T17	baseline	2.14x10 ⁻³	6	50	3.34x10 ⁻²	10	0.92	1004	103.2	237
T18							0.92	995	102.8	245
T19	less fuel	1.83x10 ⁻³					0.81	934	122.7	365
T20	more fuel	2.27x10 ⁻³					1.00	1034	124.4	157
T21	fuel @ 30 F	2.14x10 ⁻³	-1	6	3.34x10 ⁻²	10	0.92	1056	106.1	211
T22	fuel @ 70 F		21				0.92	1047	95.4	189
T23	fuel @ 90 F		32				0.92	1021	112.5	209
T24	less air		45				0.89	1051	110	128
T25	more air	58	0.9	1056	107.8	270				
T26	air @ 40 F	6	50	3.34x10 ⁻²	4	0.92	1063	114.2	211	
T27	air @ 80 F		52		27	0.92	1067	132.1	185	
T28	air @ 100 F		53		38	0.92	1026	116.4	191	

6.3.1 Baseline Test

The baseline test was conducted twice (see tests T17–T18 in table 7). The temperature map and heat flux profiles (see figures 43 and 44, respectively) show very good repeatability. The burnthrough times are listed in table 7, also showing good repeatability within the tolerance for the burnthrough times, which is ± 30 sec.

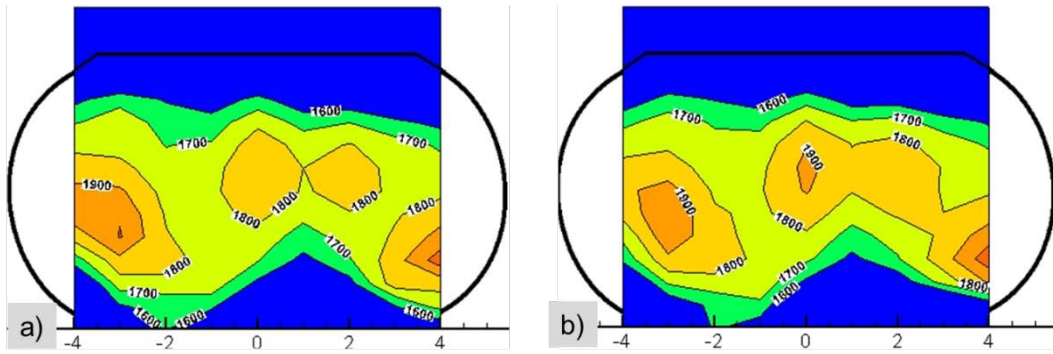


Figure 43. Temperature maps (unit °F) for baseline: a) Test T17 and b) Test T18

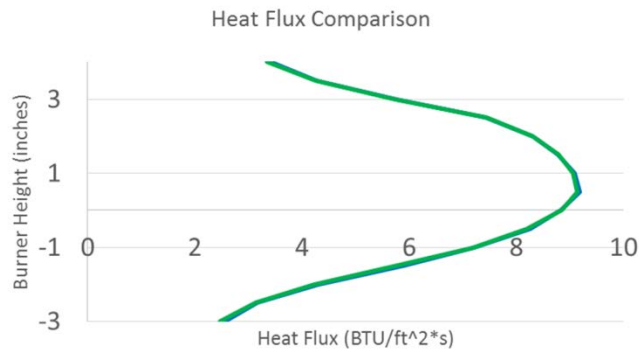
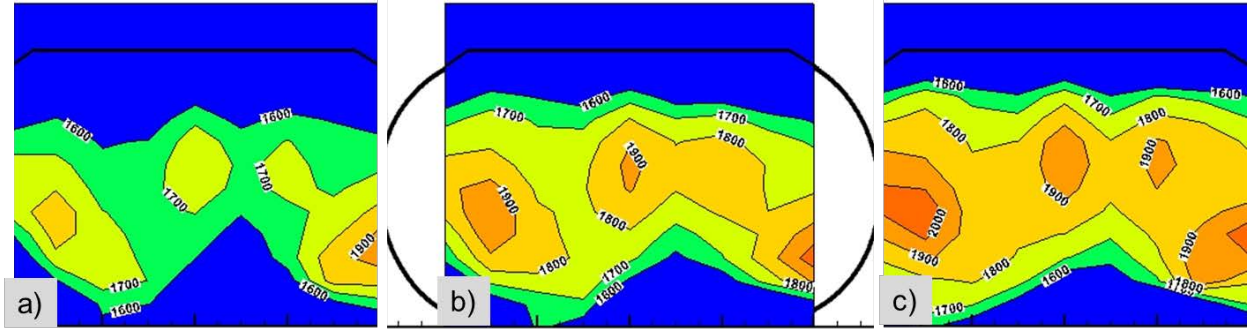


Figure 44. Heat flux profiles for the two baseline cases

6.3.2 Sensitivity to Fuel Flow Rate

Calibration and burnthrough tests were conducted at two different fuel flow rates: 10% lower and 10% higher than the baseline fuel flow rate. These test conditions are listed as tests T19 and T20 in table 7. Figure 45 shows the temperature maps for these cases compared with the baseline case (T18). It can be seen that the flame temperature increases steadily with an increase in the fuel flow rate, as expected. The burnthrough tests also indicate a clear trend, with the burnthrough times decreasing with an increase in the fuel flow rate (see figure 46). Thus, the burner becomes more severe with an increase in the fuel flow rate. Based on these results, a tolerance of $\pm 5\%$ of the baseline fuel flow rate is recommended.



**Figure 45. Effect of fuel flow rate: temperature maps (unit °F):
a) T19, less fuel, b) T18, baseline, and c) T20, more fuel**

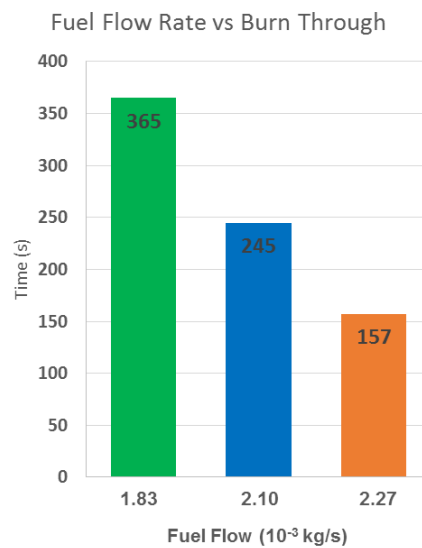


Figure 46. Effect of fuel flow rate: burnthrough

6.3.3 Sensitivity to Fuel Temperature

The effect of fuel temperature on burner performance was studied by conducting calibration maps and burnthrough tests with fuel at three different temperatures, from $-1-32^{\circ}\text{C}$ ($30-90^{\circ}\text{F}$) and comparing them with the baseline case ($6^{\circ}\text{C}/42^{\circ}\text{F}$). These tests are listed as tests T21–T23 in table 7.

The temperature maps are shown in figure 47. No clear trend can be observed among the calibration data. The burnthrough results are plotted in figure 48; no clear trend could be observed, and all times are within the tolerance for the burnthrough times.

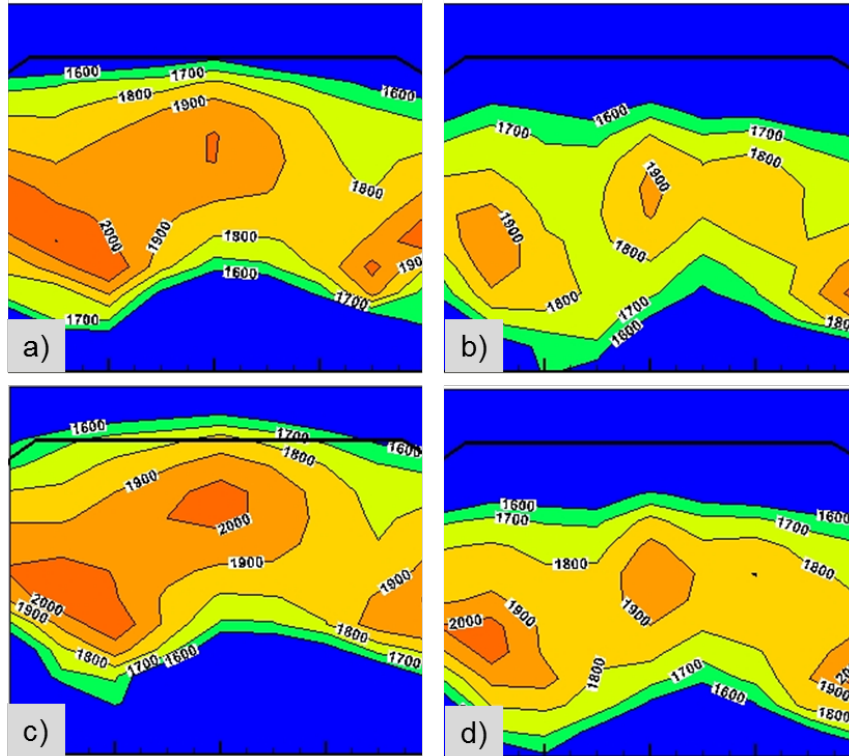


Figure 47. Effect of fuel temperature: temperature maps (unit °F): a) T21, $T_{\text{fuel}} = -1^{\circ}\text{C}$; b) T18 (baseline), $T_{\text{fuel}} = 6^{\circ}\text{C}$; c) T22, $T_{\text{fuel}} = 21^{\circ}\text{C}$; and d) T23, $T_{\text{fuel}} = 32^{\circ}\text{C}$

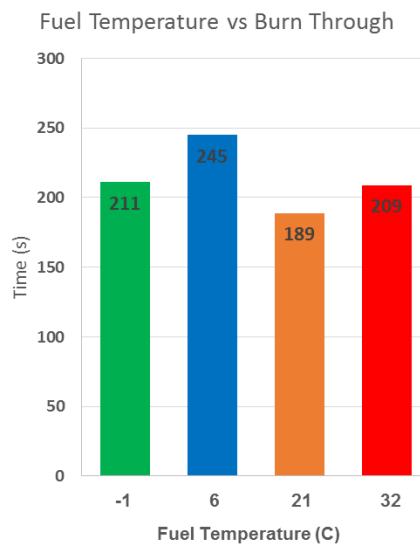
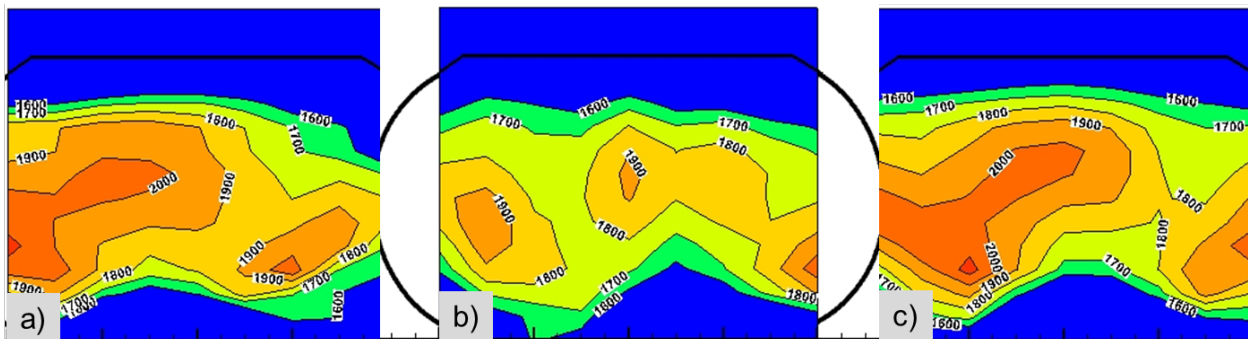


Figure 48. Effect of fuel temperature: burnthrough

6.3.4 Sensitivity to Air Mass Flow Rate

Calibration and burnthrough tests were conducted at two different air pressure settings (which changed the air mass flow rates) and were compared with the baseline case. The tests were conducted at 10% less and 10% more air mass flow rates compared with the baseline. They are listed as tests T24 and T25 in table 7. The temperature maps are shown in figure 49. The calibration temperatures for both cases seemed to be higher than that for the baseline, although this was most likely due to an issue with the baseline temperature calibration. Burnthrough times (see figure 50) do show a clear trend, increasing with an increase in the airflow rate. As the airflow rate increases, the equivalence ratio of the flame decreases; therefore, the burner is expected to become less severe, which is reflected in the burnthrough times. Similar observations were seen in section 4.3.2 for the old burner configuration. Based on these results, a tolerance of $\pm 5\%$ of the baseline air mass flow rate is recommended.



**Figure 49. Effect of airflow rate: temperature maps (unit °F):
a) T24, less air, b) T18, baseline, and c) T25, more air**

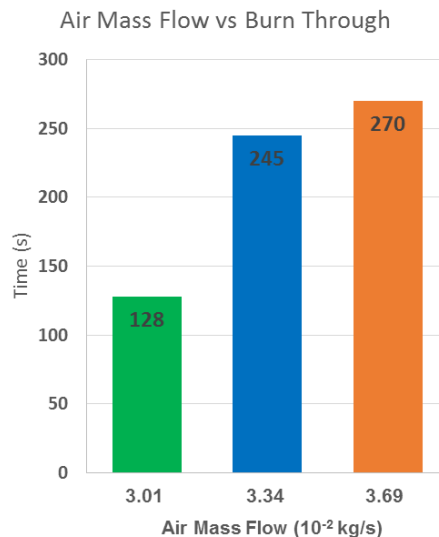


Figure 50. Effect of airflow rate: burnthrough

6.3.5 Sensitivity to Air Temperature

The effect of air temperature on burner performance was studied by conducting calibration maps and burnthrough tests with air at three different temperatures, ranging from 4°–38°C (40°–100°F) and comparing them to the baseline case (10°C, 50°F). These tests are listed as tests T26–T28 in table 7. The air pressure settings were adjusted to ensure that the air mass flow rate was constant at the different temperatures. The temperature maps are shown in figure 51. No clear trend can be observed among the calibration data. The burnthrough results are plotted in figure 52; no clear trend could be observed, and all times are within the tolerance for the burnthrough times.

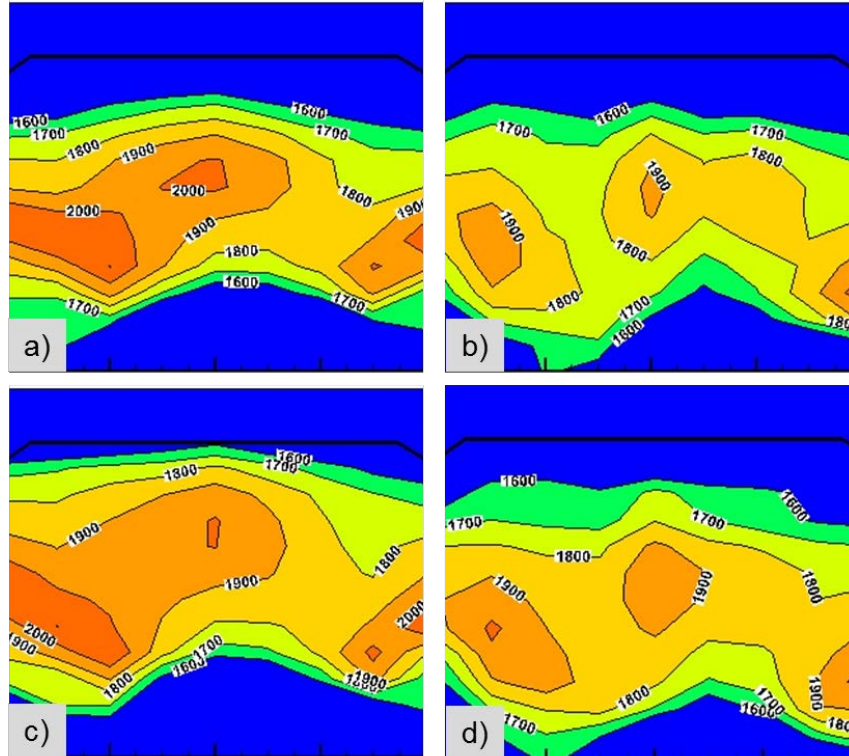


Figure 51. Effect of air temperature: temperature maps (unit °F): a) T26, $T_{\text{air}} = 4^{\circ}\text{C}$; b) T18 (baseline), $T_{\text{air}} = 10^{\circ}\text{C}$; c) T27, $T_{\text{air}} = 27^{\circ}\text{C}$; and d) T28, $T_{\text{air}} = 38^{\circ}\text{C}$

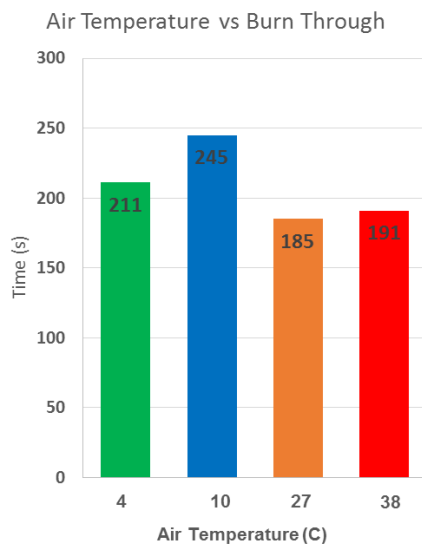


Figure 52. Effect of air temperature: burnthrough sensitivity of burner to configuration

With the intent for the NexGen burner to be calibrated on the basis of input parameters only rather than doing temperature and heat-flux calibrations, there was some concern that changes in the burner configuration, misconfiguration of the burner, or damage to some of the burner parts could affect the outcome of the fire tests because the calibrations may not be enforced. Therefore, several tests were carried out by deliberately altering the burner configuration to study the effect of these changes in the burner configuration on the performance of the burner—both calibration and burnthrough. The parameters that were changed were the distance of the fuel nozzle from the burner tube exit, the distance of the exit plane of the cone from the end of the burner tube, and the type of cone. To study the effect of damage to burner parts, the FRH was intentionally damaged by bending one of the vanes before the tests were carried out. Additional tests were desired for misaligning the fuel nozzle; however, the installation of the fuel tube made it nearly impossible to achieve this. It was concluded that it is highly improbable for the fuel nozzle to get accidentally misaligned during regular use, so these tests were discarded. Tests conducted included temperature maps and burnthrough tests using Type C panels. A rake of seven TCs was used for the temperature maps. All test conditions are listed in table 8.

Table 8. Test conditions for impact of burner configuration

Test Case	Description	Fuel		Air			Φ	Avg T	Heat Flux	Burnthrough Time
		kg/s	°C	psi g	kg/s	°C		°C	kW/m ²	sec
T29	Baseline	2.13 $\times 10^{-3}$	6	50	3.34×10^{-2}	10	0.94	1038	115.8	190
T30								1043	126.1	184
T31								1013	124.9	163
T32								1024	135.1	183
T33								1013	130.6	163
T34								1019	132.9	160
T35	Nozzle @ -12.7							1027	113.6	170
T36								1021	93.1	182
T37	Nozzle @ +12.7							1038	119.2	206
T38								1029	123.8	206
T39	Cone @ -50.8							1036	129.5	162
T40	Cone @ -25.4							1042	121.5	180
T41	Cone @ +25.4							1049	96.5	206
T42	Cone @ +50.8							1010	115.8	221
T43	Ceramic insulated cone							1047	121.5	162
T44								1057	131.7	163
T45	Inconel cone							1032	126.1	143
T46								1012	129.5	136
T47	FAA cone design							1032	93.1	165
T48								1031	114.7	152
T49	Slightly deformed FRH	938	123.8	170						
T50		991	127.2	172						
T51	Severely deformed FRH	1005	115.8	154						
T52		979	106.8	181						

6.3.6 Baseline

New baseline cases were tested. Because the burnthrough times were different from the baseline times reported in section 6.3.1, the test was repeated several times on different days. The test conditions are reported as tests T29–T34 in table 8. It was concluded that the issue was more likely

with the burnthrough results from section 6.3.1 because the current results compared favorably with all the other tests reported in section 6.3. Figure 53 shows the temperature map for the baseline case, also indicating the region of the burner that was studied for this set of tests. Figure 54 plots the burnthrough times for the baseline tests, including results from section 6.3.

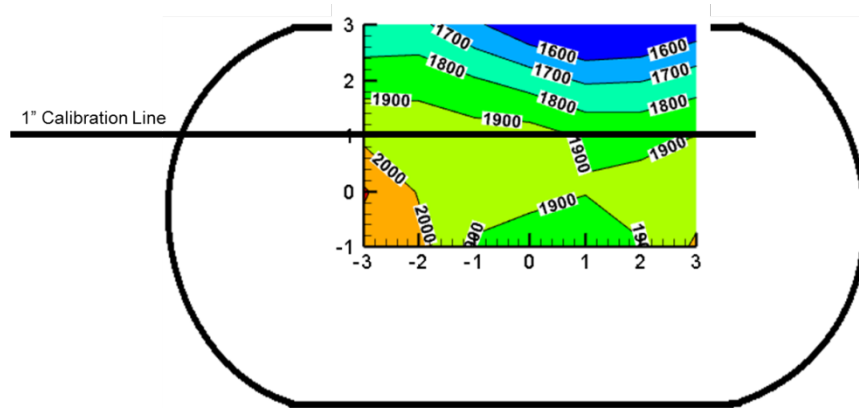


Figure 53. Baseline temperature map, indicating region being tested

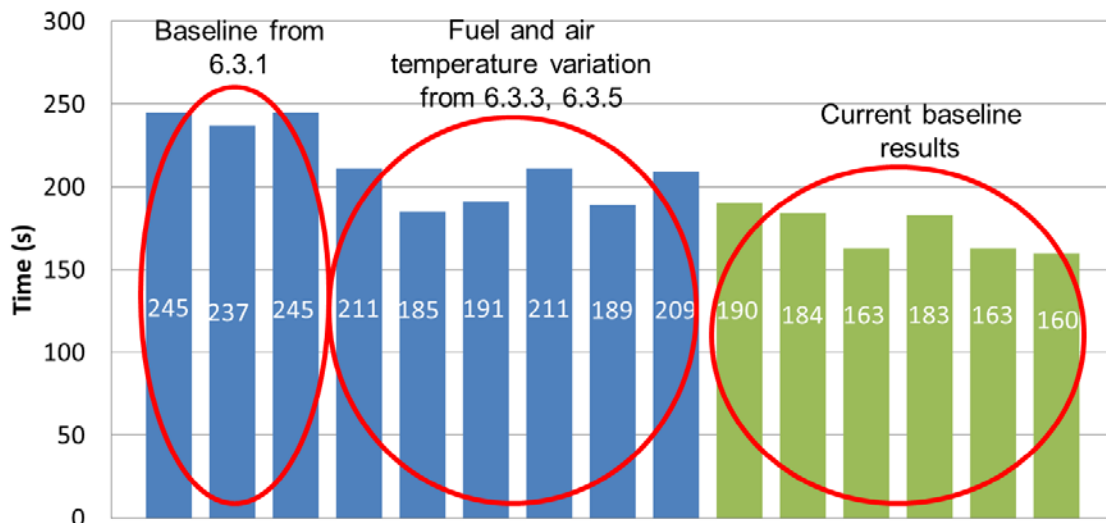


Figure 54. Baseline burnthrough times

6.3.7 Effect of Fuel-Nozzle Depth

For the baseline burner configuration, the fuel nozzle is located at a distance of 28.6 mm (1.125 in.) behind the end of the burner tube. The effect of fuel-nozzle depth was studied by varying this distance by ± 12.7 mm (± 0.5 in.), with each condition repeated twice. The test conditions are listed as tests T35–T38 in table 8. Figure 55 shows the temperature maps for the two depths compared with the baseline case, along with schematics of the nozzle locations. There was no significant difference in the temperature distribution for the two cases. Figure 56 shows the burnthrough times for the different fuel-nozzle positions. It can be observed that moving the fuel nozzle does have a

slight impact on the burnthrough time—the time increased as the distance of the nozzle increased—so the severity of the burner decreased as the nozzle was moved further back from the burner tube exit. However, the amount of change in the burnthrough time was small; all burnthrough times were still within the tolerance for the baseline case. Therefore, the results of these tests were inconclusive, although they do indicate the need to establish a tolerance on the fuel-nozzle depth. A tolerance of ± 6.4 mm (0.25 in.) was recommended based on these results.

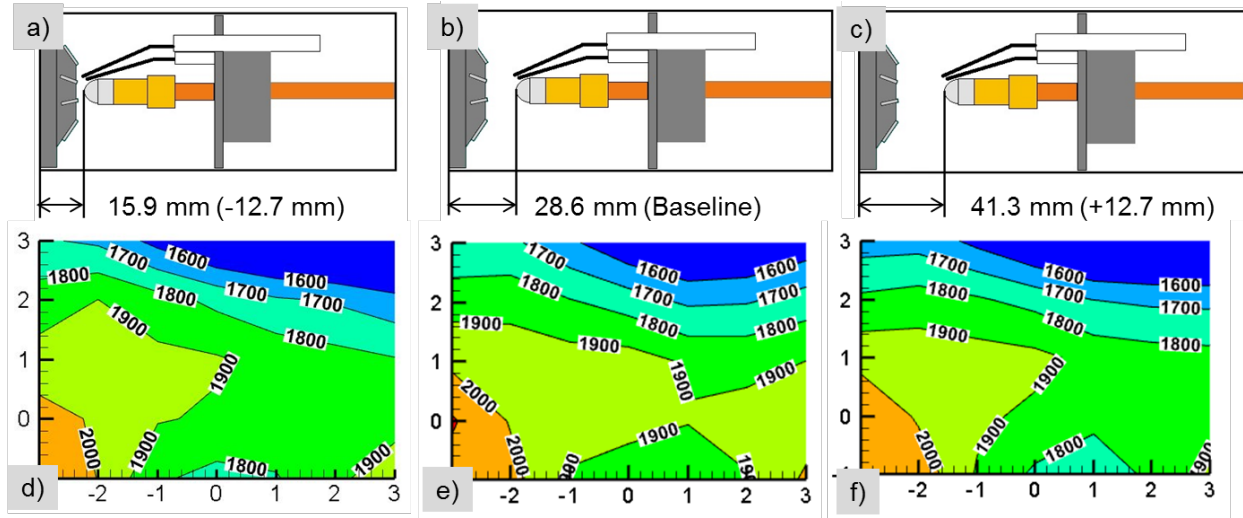


Figure 55. Effect of fuel-nozzle depth: temperature maps (unit °F): a) -12.7 mm, b) baseline, c) +12.7 mm, d) map for -12.7 mm; e) map for baseline, and f) map for +12.7 mm

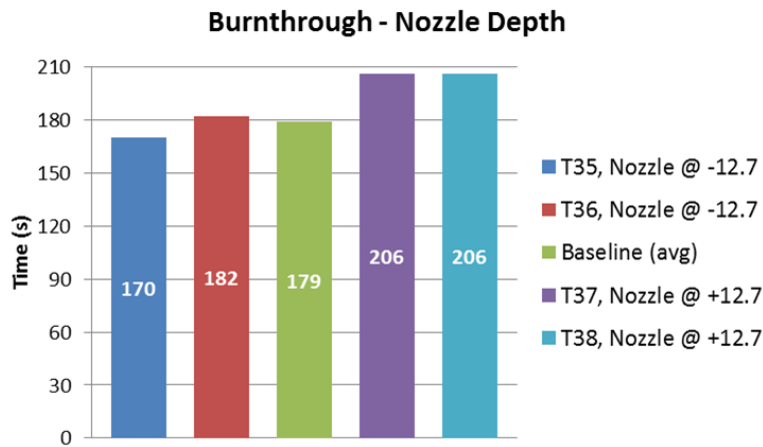


Figure 56. Effect of nozzle depth: burnthrough

6.3.8 Effect of Cone Depth

For the baseline burner configuration, the expansion of the cone starts at the end of the burner tube, with a circular sleeve wrapped around the burner tube. However, during installation or service, it is possible to accidentally mislocate the cone. Therefore, tests were conducted by moving the burner cone forward and back at locations of ± 50.8 mm (± 2 in.) and ± 25.4 mm (± 1 in.). The test conditions

are listed as tests T39–T42 in table 8. Figure 57 shows a schematic of the cone locations and the temperature maps for the different cone depths. The cone depth had no significant effect on the calibration temperature. The burnthrough results are shown in figure 58. A clear trend is observed for the burnthrough times, which increases as the cone moves forward. The test panel is now always located at 101.6 mm (4 in.) from the end of the burner cone. Moving the cone forward increases the distance from the end of the burner tube to the test location and causes the burner to be less severe. Therefore, there is a need to establish a tolerance for the burner cone depth. Based on these results, a tolerance of ± 25.4 mm (± 1 in.) is recommended.

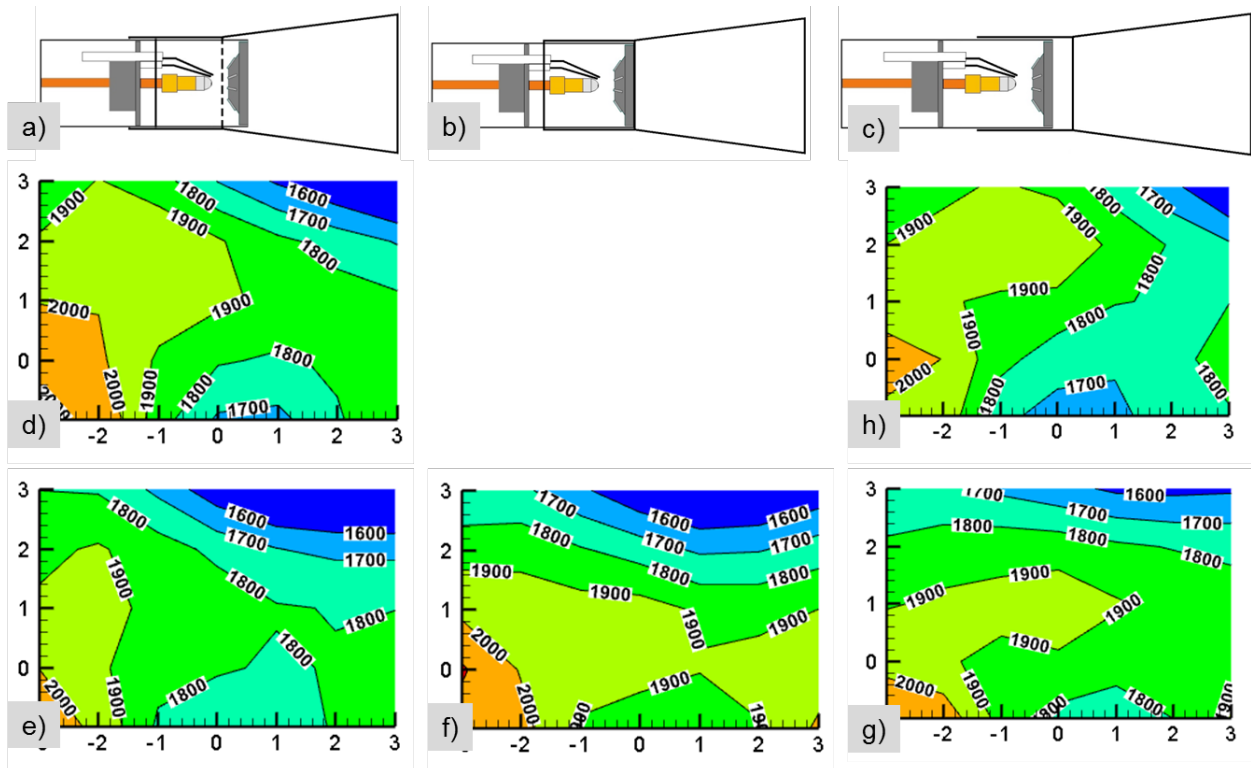


Figure 57. Effect of cone depth: temperature maps (unit °F): a) cone moved back, b) baseline, c) cone moved forward, d) map for -50.8 mm, e) map for -25.4 mm, f) map for baseline, g) map for + 25.4 mm, and h) map for +50.8 mm

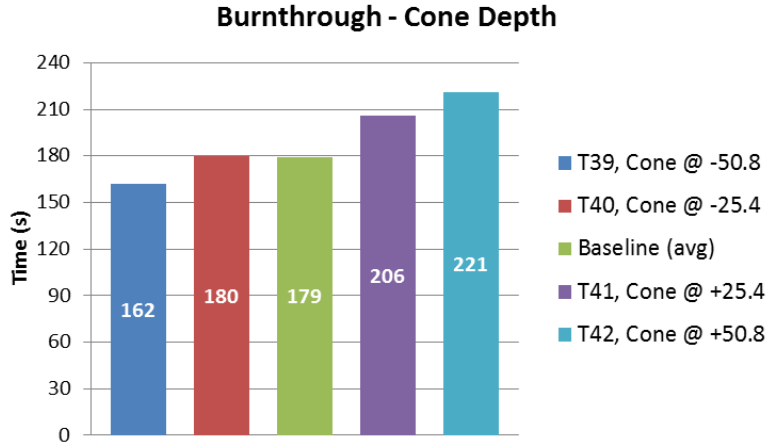


Figure 58. Effect of cone depth: burnthrough

6.3.9 Effect of Cone Type

The impact of cone material, design, and construction was studied by using three different cone designs and was compared with the baseline cone. The cone designs are shown in figure 59. The baseline cone was made of SS and was a one-piece construction with a 152.4 mm (6 in.) long straight section at the upstream end. Two other cones were variations of the baseline cone: 1) a stainless steel cone coated with a high-temperature ceramic insulation on the outside, and 2) a cone made from Inconel[®]. The fourth type was the one being used at the FAA Tech Center and features a two-piece stainless steel cone design welded together downstream of the burner tube with bolts on the sides of the straight section to clamp them on to the burner tube. The test conditions are listed as tests T43–T48 in table 8.

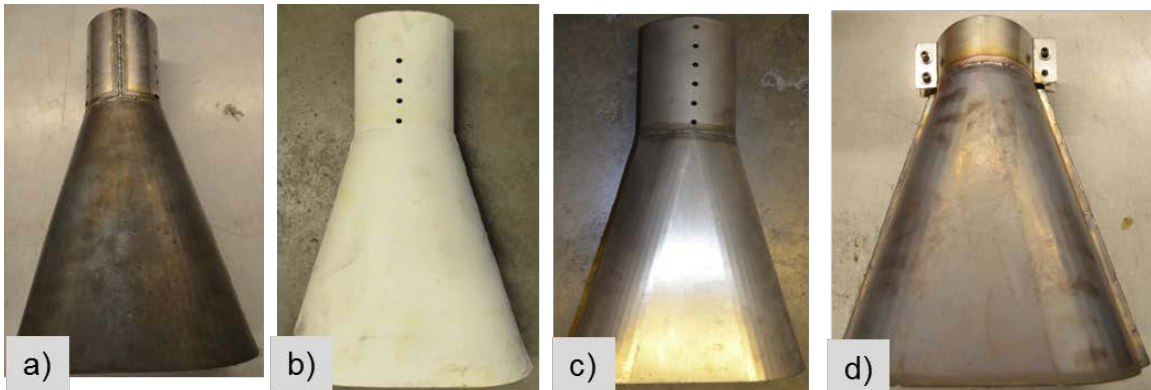


Figure 59. Different cone types: a) baseline (stainless steel), b) ceramic insulated, c) Inconel, and d) FAA design (stainless steel)

Figure 60 shows the temperature maps for the different cones. There was no major difference between the cones, although there was some difference in the locations of the high-temperature areas. Burnthrough tests were conducted using the different cone designs, and the burnthrough times (see figure 61) were similar for three of the cone designs. The only exception was the Inconel cone, which had a lower burnthrough time compared with the other three, indicating that the flame

was more severe using this cone. Therefore, it is recommended that the material, design, and construction of the burner cone should be properly defined and documented.

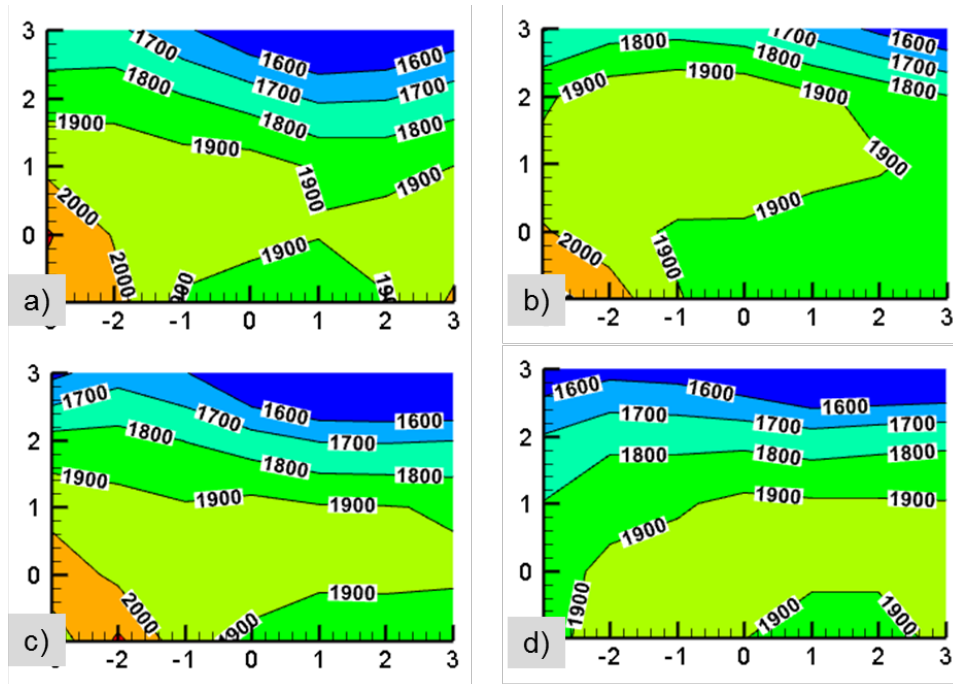


Figure 60. Effect of cone type: temperature maps (unit °F): a) baseline (stainless steel) cone, b) ceramic-coated stainless steel cone, c) Inconel cone, and d) FAA design (stainless steel) cone

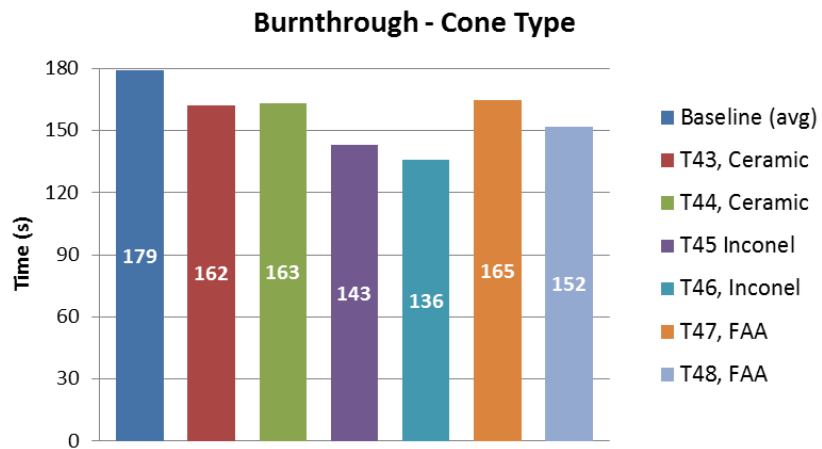


Figure 61. Effect of cone type: burnthrough

6.3.10 Effect of FRH deformation

Tests were conducted to simulate accidental damage after intentionally deforming the FRH. The deformation was caused by bending one of the metal tabs on the outside and one of the swirl vanes on the inside. The test conditions for the deformed FRH are listed as tests T49–T52 in table 8. Figure 62 shows pictures of the deformed FRH compared with the baseline. Figure 63 shows the temperature maps for the baseline and the deformed FRHs. The overall distributions look similar, although there are small differences in the locations of the max temperatures. Figure 64 plots the burnthrough times for these cases, and it can be seen that the deformation of the FRH did not have a significant impact on the burnthrough times because all were within the tolerance.



Figure 62. Deformation of FRH: a) baseline (undamaged), b) slightly deformed, and c) severely deformed

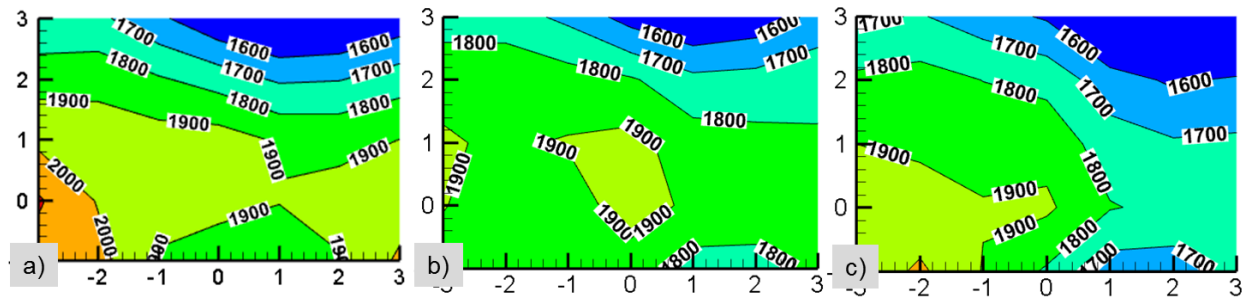


Figure 63. Effect of FRH deformation: temperature maps (unit °F): a) baseline (undamaged), b) slightly deformed, and c) severely deformed

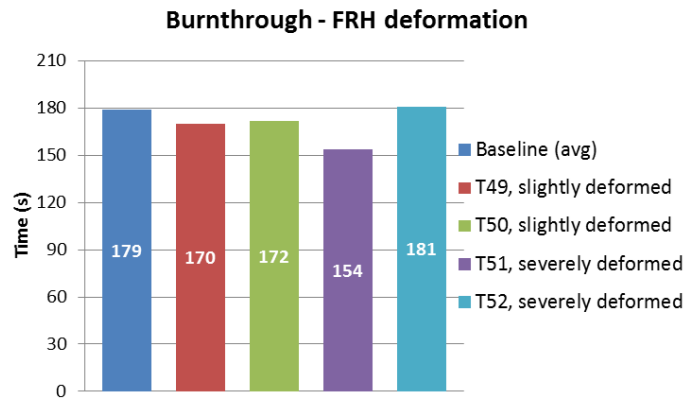


Figure 64. Effect of FRH deformation: burnthrough

7. SUMMARY AND CONCLUSIONS

An experimental study has been conducted to assist the FAA in understanding the performance of the NexGen burner and provide the benchmark to adapt the burner settings for future use. The NexGen burner was found to be suitable for use in power-plant fire tests.

A previous study [8], conducted as a part of the same grant, focused on the original NexGen burner configuration, consisting of the stator and turbulator. During this study, it was discovered that insufficient specificity in the standards could allow significant differences in the burner calibration, which could lead to differences in test results and reduce repeatability of results. The effect of the size of thermocouples used for temperature calibration was studied and was observed to have a significant impact on the test results. The effects of burner operating parameters, air and fuel flow, and the effect of test panel size were studied in the previous work.

The current study continued the research on the original NexGen burner configuration and on the updated NexGen burner configuration consisting of the flame retention head (FRH) and the Delavan fuel nozzle. For the original configuration, the effects of burner orientation and of fuel and air temperature were studied. For the updated configuration, before selecting the configuration selected by the FAA, initial tests were conducted to study the properties of the different FRHs and fuel nozzles, consisting of the F31 FRH and the 2.5 GPH W fuel nozzle. Tests were conducted to study the effect of burner operating conditions on burner calibration and burnthrough test results. Operating conditions studied included fuel and air-mass flow rates and temperatures. Additionally, tests were conducted to study the effect of changes to the burner configuration. These tests were conducted to understand the effect of accidental changes to the burner configuration on test results. Parameters tested included the location of the fuel nozzle, the location of the cone, the material and design of the cone, and damage to the FRH. For the parameters that did have significant impact on the burner performance, tolerances were recommended to ensure repeatability of test results.

The recommendations are as follows:

1. A tolerance of $\pm 5\%$ of the defined fuel flow rate is recommended.
2. Air mass flow should be regulated. A tolerance of $\pm 5\%$ of the defined air mass flow rate should be applied.
3. If air temperature changes, care should be taken to ensure that the air mass flow rate is held constant by adjusting the pressure setting.
4. For the fuel nozzle depth relative to the burner tube exit, a tolerance of ± 6.4 mm (0.25 in.) is recommended.
5. For the location of the burner cone relative to the burner tube exit, a tolerance of ± 25.4 mm (1 in.) is recommended.
6. The material and design of the cone should be defined in the standards.
7. A change in burner inclination is observed to have an impact on the test results. Operating settings should be prescribed for different burner inclinations.

8. REFERENCES

1. Definitions and Abbreviations, 14 CFR § 1 (1966). Retrieved from <http://www.ecfr.gov/cgi-bin/retrieveECFR?gp=&SID=d7779543dd5a739007e20fa1d087ecb0&mc=true&n=pt14.1.1&r=PART&ty=HTML>.
2. Airworthiness Standards: Transport Category Airplanes, 14 CFR § 25 (1964). Retrieved from <http://www.ecfr.gov/cgi-bin/text-idx?SID=f31ec0e22b17acd87b72e0609c22eb8a&mc=true&node=pt14.1.25&rgn=div5>.
3. Airworthiness Standards: Aircraft Engines, 14 CFR § 33 (1966). Retrieved from <http://www.ecfr.gov/cgi-bin/text-idx?SID=f31ec0e22b17acd87b72e0609c22eb8a&mc=true&node=pt14.1.33&rgn=div5>.
4. FAA. (1990, February). Advisory Circular 20-135. *Powerplant Installation and Propulsion System Component Fire Protection Test Methods, Standards, and Criteria*. Retrieved from https://www.faa.gov/regulations_policies/advisory_circulars/index.cfm/go/document.information/documentID/22194
5. *Federal Aviation Administration, "FAA Power Plant Engineering Report No. 3A: Standard Fire Test Apparatus and Procedure (For Flexible Hose Assemblies),"* March, 1978. Retrieved from <https://www.fire.tc.faa.gov/pdf/faa3-A.pdf>
6. ISO 2685:1998: Aircraft—Environmental Test Procedure for Airborne Equipment—Resistance to Fire in Designated Fire Zones.
7. FAA. (2009, August). Advisory Circular 33.17-1A. *Engine Fire Protection*. Retrieved from https://www.faa.gov/regulations_policies/advisory_circulars/index.cfm/go/document.information/documentID/99608
8. FAA Report. (2015). Development of Next Generation Burner Characteristics for Fire Testing of Power Plant Materials and Components. (DOT/FAA/TC-13/38).
9. FAA Report. (2009). Development of a Next-Generation Burner for Use in Testing Thermal Acoustic Insulation Burnthrough Resistance. (DOT/FAA/AR-TN09/23).
10. Ochs, R. (2009). *NexGen burner for seat cushion fire testing*. Paper presented at the International Aircraft Materials Fire Test Working Group, Atlantic City, NJ. Retrieved from <https://www.fire.tc.faa.gov/pdf/materials/Oct09Meeting/Ochs-1009-SEATS.pdf>

11. Salter, T. (2011). *Seat cushion test method update*. Paper presented at the International Aircraft Materials Fire Test Working Group, Atlantic City, NJ. Retrieved from https://www.fire.tc.faa.gov/pdf/materials/.../Salter-1011-Seat_Cushion_Test.pdf
12. Summer, S. (2013). *Next generation fire test burner for powerplant fire testing applications*. Paper presented at the International Aircraft Systems Fire Protection Working Group, Bremen, Germany. Retrieved from <https://www.fire.tc.faa.gov/pdf/systems/May13Meeting/Hill-0513-StatusNexGenBurnerPowerplantTesting.pdf>.
13. Hill, R. (2012). *Seat cushion test method update*. Paper presented at the International Aircraft Materials Fire Test Working Group, Singapore. Retrieved from <https://www.fire.tc.faa.gov/pdf/materials/Feb12Meeting/Hill-0212-SeatCushion.pdf>.
14. Marker, T. (2012). *Task group session on revised cargo liner test*. Paper presented at the International Aircraft Materials Fire Test Working Group, Singapore. Retrieved from <https://www.fire.tc.faa.gov/ppt/materials/Feb12Meeting/marker-0212cargotask.ppt>.
15. Salter, T. (2013). *Seat cushion test method update*. Paper presented at the International Aircraft Materials Fire Test Working Group, Manchester, UK. Retrieved from <https://www.fire.tc.faa.gov/pdf/materials/June13Meeting/Marker-0613-SeatCushion.pdf>.
16. Ochs, R. I. (2010). *Development of the next generation fire test burner for powerplant fire testing applications*. Paper presented at the International Aircraft Systems Fire Protection Working Group, London, UK. Retrieved from <https://www.fire.tc.faa.gov/pdf/systems/May10Meeting/ochs-0510-DevOfNexGenForPowerplantTest.pdf>.

APPENDIX A—TABLES FROM PREVIOUS WORK [8]

Table A-1. Effect of turbulator modification on burner calibration

Turbulator	JetA		Air		Φ	Avg T		Heat Flux		Std Deviation
	GPH	kg/s	scfm	kg/s		°F	°C	BTU/ft ² -s	kW/m ²	°C
Original	3.04	0.00259	61	0.0341	1.11	2025	1107.2	11.14	126.5	40.4
Modified	2.85	0.00243	61	0.0341	1.05	2009	1098.3	10.54	119.7	32.7

Table A-2. Effect of calibration TC size on burner calibration

TC	JetA		Air		Φ	Avg T		Heat Flux	
	GPH	kg/s	scfm	kg/s		°F	°C	BTU/ft ² -s	kW/m ²
Baseline (1/8 in.)	2.44	2.08 x 10 ⁻³	55.2	3.08 x 10 ⁻²	0.99	2007	1097	9.74	110.6
Smaller (1/16 in.)	2.35	2.00 x 10 ⁻³	55.2	3.08 x 10 ⁻²	0.95	2021	1105	9.43	107.1

Table A-3. Calibration-only trials

Calibration Trial	Jet-A		Air		Total Flow Rate	Φ	Avg T		Heat Flux		Comments
	GPH	kg/s	scfm	kg/s	kg/s		°F	°C	BTU/ft ² -s	kW/m ²	
Case #1	1.83	1.56 x 10 ⁻³	63.9	3.58 x 10 ⁻²		0.64	1690	921	6.82	77.45	Sensitivity to fuel flow
Case #2	1.96	1.67 x 10 ⁻³				0.69	1763	962	7.44	84.53	
Case #3	2.09	1.78 x 10 ⁻³				0.73	1835	1002	8.03	91.2	
Case #4	2.22	1.89 x 10 ⁻³				0.78	1878	1026	8.76	99.51	
Case #5	2.34	2.00 x 10 ⁻³				0.82	1951	1066	9.93	112.73	
Case #6	2.43	2.07 x 10 ⁻³				0.85	2018	1104	11.06	125.62	
Case #7	2.6	2.22 x 10 ⁻³				0.91	2015	1102	11.17	126.86	
Case #8	2.73	2.33 x 10 ⁻³				0.96	2065	1130	11.96	135.88	
Case #9	2.86	2.43 x 10 ⁻³				1	2085	1141	12.00	136.28	
Case #10	2.34	2.00 x 10 ⁻³	55.3	3.09 x 10 ⁻²		0.95	1892	1033	9.93	112.83	Sensitivity to airflow
Case #11			58	3.24 x 10 ⁻²		0.91	1938	1059	9.29	105.54	
Case #12			61	3.41 x 10 ⁻²		0.86	1948	1064	9.08	103.16	
Case #13			63.9	3.58 x 10 ⁻²		0.82	1943	1062	9.28	105.4	
Case #14			66.8	3.73 x 10 ⁻²		0.79	1909	1043	9.75	110.78	
Case #15			69.6	3.89 x 10 ⁻²		0.75	1881	1027	9.57	108.69	

Table A-3. Calibration-only trials (continued)

Calibration Trial	Jet-A		Air		Total Flow Rate	Φ	Avg T		Heat Flux		Comments
	GPH	kg/s	scfm	kg/s	kg/s		°F	°C	BTU/ft ² -s	kW/m ²	
Case #16	1.47	1.25 x 10 ⁻³	47.6	2.66 x 10 ⁻²	2.78 x 10 ⁻²	0.69	1651	899	6.74	76.58	Sensitivity to total flow rate
Case #17	1.6	1.36 x 10 ⁻³	51.6	2.88 x 10 ⁻²	3.01 x 10 ⁻²		1727	942	7.53	85.58	
Case #18	1.68	1.43 x 10 ⁻³	54.4	3.04 x 10 ⁻²	3.18 x 10 ⁻²		1764	962	7.91	89.83	
Case #19	1.77	1.51 x 10 ⁻³	57.3	3.20 x 10 ⁻²	3.35 x 10 ⁻²		1781	972	8.39	95.34	
Case #20	1.89	1.61 x 10 ⁻³	61.2	3.42 x 10 ⁻²	3.59 x 10 ⁻²		1812	989	8.74	99.25	
Case #21	2	1.71 x 10 ⁻³	65.2	3.64 x 10 ⁻²	3.81 x 10 ⁻²		1863	1017	9.48	107.7	
Case #22	1.62	1.38 x 10 ⁻³	47.6	2.66 x 10 ⁻²	2.80 x 10 ⁻²	0.76	1723	939	7.72	87.7	
Case #23	1.73	1.47 x 10 ⁻³	51.2	2.86 x 10 ⁻²	3.00 x 10 ⁻²		1752	956	8.14	92.52	
Case #24	1.84	1.57 x 10 ⁻³	54.4	3.04 x 10 ⁻²	3.20 x 10 ⁻²		1816	991	9.04	102.68	
Case #25	1.96	1.67 x 10 ⁻³	57.8	3.23 x 10 ⁻²	3.40 x 10 ⁻²		1836	1002	9.03	102.55	
Case #26	2.08	1.77 x 10 ⁻³	61.2	3.42 x 10 ⁻²	3.60 x 10 ⁻²		1854	1012	9.37	106.4	
Case #27	2.14	1.82 x 10 ⁻³	63	3.52 x 10 ⁻²	3.70 x 10 ⁻²		1897	1036	9.90	112.47	
Case #28	2.2	1.87 x 10 ⁻³	64.8	3.62 x 10 ⁻²	3.81 x 10 ⁻²		1914	1046	10.20	115.88	
Case #29	2.25	1.92 x 10 ⁻³	66.6	3.72 x 10 ⁻²	3.91 x 10 ⁻²	1922	1050	10.04	114.06		
Case #30	1.83	1.56 x 10 ⁻³	47.8	2.67 x 10 ⁻²	2.83 x 10 ⁻²	0.86	1884	1029	8.68	98.54	
Case #31	1.96	1.67 x 10 ⁻³	51	2.85 x 10 ⁻²	3.02 x 10 ⁻²		1859	1015	8.81	100.01	
Case #32	2.09	1.78 x 10 ⁻³	54.6	3.05 x 10 ⁻²	3.23 x 10 ⁻²		1948	1064	10.48	119.06	

A-3

Table A-3. Calibration-only trials (continued)

Calibration Trial	Jet-A		Air		Total Flow Rate	Φ	Avg T		Heat Flux		Comments
	GPH	kg/s	scfm	kg/s	kg/s		°F	°C	BTU/ft ² -s	kW/m ²	
Case #33	2.22	1.89 x 10 ⁻³	58	3.24 x 10 ⁻²	3.43 x 10 ⁻²		1992	1089	10.64	120.82	
Case #34	2.35	2.00 x 10 ⁻³	61.2	3.42 x 10 ⁻²	3.62 x 10 ⁻²		2049	1121	11.46	130.19	
Case #35	2.48	2.11 x 10 ⁻³	64.6	3.61 x 10 ⁻²	3.82 x 10 ⁻²		2075	1135	11.86	134.66	
Case #36	2.61	2.22 x 10 ⁻³	68	3.80 x 10 ⁻²	4.02 x 10 ⁻²		2088	1142	12.25	139.12	
Case #37	2.05	1.75 x 10 ⁻³	49.9	2.79 x 10 ⁻²	2.97 x 10 ⁻²	0.92	1899	1037	9.82	111.49	
Case #38	2.2	1.87 x 10 ⁻³	53.5	2.99 x 10 ⁻²	3.18 x 10 ⁻²		1972	1078	9.80	111.32	
Case #39	2.35	2.00 x 10 ⁻³	56.9	3.18 x 10 ⁻²	3.38 x 10 ⁻²		1975	1079	10.11	114.79	
Case #40	2.49	2.12 x 10 ⁻³	60.3	3.37 x 10 ⁻²	3.59 x 10 ⁻²		2004	1096	12.07	137.1	
Case #41	2.63	2.24 x 10 ⁻³	63.9	3.57 x 10 ⁻²	3.80 x 10 ⁻²		2031	1111	12.02	136.49	

Table A-4. Burnthrough test cases

Test Case	Test Sample	Test Description	Jet-A		Air		Φ	Avg T		Heat Flux		Burnthrough Time
			GPH	kg/s	scfm	kg/s		°F	°C	BTU/ft ² -s	kW/m ²	min
Test #1	A	Fuel Leaner	2.2	1.88x10 ⁻³	67.6	3.78x10 ⁻²	0.74	1936	1058	9.24	104.9	
Test #2								1951	1066	9.33	106	
Test #3		Baseline	2.25	1.92x10 ⁻³	64.0	3.58x10 ⁻²	0.8	1950	1066	9.13	103.7	
Test #4								1923	1051	9.03	102.6	
Test #5		Fuel Richer	2.25	1.92x10 ⁻³	58.6	3.27x10 ⁻²	0.87	1951	1066	9.33	106	17
Test #6								1923	1050	9.03	102.6	17
Test #7	B	Fuel Leaner	2.25	1.92x10 ⁻³	67.6	3.78x10 ⁻²	0.76	1920	1049	9.43	107.1	15
Test #8								1920	1049	9.43	107.1	
Test #9		Baseline	2.25	1.92x10 ⁻³	62.2	3.47x10 ⁻²	0.82	1920	1049	9.54	108.3	11.5
Test #10								1920	1049	9.43	107.1	
Test #11		Fuel Richer	2.25	1.92x10 ⁻³	57.7	3.22x10 ⁻²	0.88	1937	1059	9.54	108.3	10
Test #12								1926	1052	9.54	108.3	10
Test #13		Small TCs	2.14	1.83x10 ⁻³	60.4	3.37x10 ⁻²	0.82	1908	1042	9.03	102.6	
Test #14								1919	1048	9.03	102.6	

APPENDIX B—DETAILED TABLES FOR CURRENT WORK

Table B-1. Detailed test conditions for impact of burner orientation (baseline configuration)

Test Case	Orientation	Calibration Offset	Jet-A		Air		Φ	Avg T		Heat Flux		Burnthrough Time	
			GPH	kg/s	scfm	kg/s		°F	°C	BTU/ft ² -s	kW/m ²	sec	
T1	0°	1 in.	2.25	1.92x10 ⁻³	67.6	3.78x10 ⁻²	0.76	1920	1049	9.4	106.8	900	
T2								1920	1049	9.4	106.8		
T3	15°		2.36	2.01x10 ⁻³	66.7	3.74x10 ⁻²	0.81	1922	1050	10.3	117	640	
T4								1921	1049	10.4	118.1		
T5	30°		2.55	2.17x10 ⁻³	66.7	3.74x10 ⁻²	0.87	1928	1053	11	124.9	550	
T6								1930	1054	11.1	126.1	570	
T7	45°		2.61	2.22x10 ⁻³	66.7	3.74x10 ⁻²	0.89	1929	1054	11.4	129.5	600	
T8								1920	1049	11.5	130.6	580	
T9	45°		No offset	2.52	2.15x10 ⁻³	66.7	3.74x10 ⁻²	0.86	1912	1044	11.1	126.1	750
T10									1916	1047	11.2	127.2	730

B-1

Table B-2. Detailed test conditions for impact of fuel temperature on burner calibration (baseline configuration)

Test Case	Jet-A				Air			Φ	Avg T		Heat Flux	
	GPH	kg/s	°F	°C	psig	scfm	kg/s		°F	°C	BTU/ft ² -s	kW/m ²
C1	2.51	2.14x10 ⁻³	59	15	60	66.7	3.74x10 ⁻²	0.84	1954	1068	10.53	119.6
C2			92	33					1972	1078	10.45	118.7
C3			102	39					1980	1082	10.57	120
C4			125	52					1982	1083	10.61	120.5
C5	2.78	2.37x10 ⁻³	59	15				0.93	2044	1118	11.48	130.4
C6			92	33					2051	1122	11.8	134
C7			102	39					2067	1131	11.86	134.7
C8			125	52					2070	1132	11.52	130.8

Table B-3. Detailed test conditions for impact of air temperature on burner calibration (baseline configuration)

Test Case	Fuel		Air					Φ	Avg T		Heat Flux	
	GPH	kg/s	psig	scfm	kg/s	°F	°C		°F	°C	BTU/ft ² -s	kW/m ²
C9	2.51	2.14x10 ⁻³	60	65.8	3.69x10 ⁻²	62	17	0.85	1918	1048	10.35	117.5
C10				64.3	3.60x10 ⁻²	88	31	0.87	1932	1056	10.44	118.6
C11				62.6	3.51x10 ⁻²	117	47	0.9	1943	1062	10.39	118
C12				61.6	3.45x10 ⁻²	137	58	0.91	1963	1073	10.63	120.7
C13	2.78	2.37x10 ⁻³		65.8	3.69x10 ⁻²	62	17	0.94	2020	1104	11.43	129.8
C14				64.3	3.60x10 ⁻²	88	31	0.97	2031	1111	11.73	133.2
C15				62.6	3.51x10 ⁻²	117	47	0.99	2047	1119	11.64	132.2
C16				61.6	3.45x10 ⁻²	137	58	1.01	2059	1126	11.92	135.4

Table B-4. Detailed test conditions for impact of air temperature on burnthrough results (baseline configuration)

Test Case	Description	Fuel		Air					Φ	Avg T		Heat Flux		Burnthrough time
		GPH	kg/s	psig	scfm	kg/s	°F	°C		°F	°C	BTU/ft ² -s	kW/m ²	sec
T11	cold @ 60 psi	2.62	2.23 x10 ⁻³	60	64.6	3.62x10 ⁻²	82	28	0.91	2013	1101	11.46	130.1	610
T12					64.9	3.64x10 ⁻²	78	26	0.9	2008	1098	11.37	129.1	600
T13	hot @ 60 psi				61.7	3.46x10 ⁻²	134	57	0.95	2009	1098	11.52	130.8	540
T14					61.4	3.44x10 ⁻²	140	60	0.95	2021	1105	11.58	131.5	510
T15	cold @ 57 psi			57	62.1	3.48x10 ⁻²	81	27	0.94	2006	1097	11.54	131.1	520
T16					62.3	3.49x10 ⁻²	77	25	0.94	2008	1098	11.38	129.2	540

Table B-5. Detailed test conditions for impact of FRH and fuel nozzle (updated configuration)

Test Case	FRH	Fuel Nozzle	Fuel		Air			Φ	Avg T		Heat Flux	
			GPH	kg/s	psig	scfm	kg/s		°F	°C	BTU/ft ² -s	kW/m ²
C17	F22	2.0	1.85	1.58x10 ⁻³	60	65	3.64x10 ⁻²	0.64	1620	882	9.5	107.9
C18	F31	2.0							1732	944	10.9	123.8
C19	F12	2.25	2.1	1.79x10 ⁻³				0.72	1752	956	12.4	140.8
C20	F22	2.25							1777	969	12	136.3
C21	F31	2.25						1834	1001	12.2	138.5	
C22	F22	2.5	2.3	1.96x10 ⁻³				0.79	1843	1006	13.8	156.7
C23	F31	2.5			1871	1022	14		159			

Table B-6. Detailed test conditions for impact of burner operating conditions (updated configuration)

Test Case	Description	Fuel					Air					Φ	Avg T		Heat Flux		Burnthrough Time		
		psi	GPH	kg/s	°F	°C	psig	pph	kg/s	°F	°C		°F	°C	BTU/ft ² -s	kW/m ²		sec	
T17	baseline	105	2.46	2.10 x10 ⁻³	42	6	50	265	3.34 x10 ⁻²	50	10	0.92	1840	1004	9.09	103.2	237		
T18												0.92	1823	995	9.05	102.8	245		
T19	less fuel	80	2.15	1.83 x10 ⁻³	42	6	50	265	3.34 x10 ⁻²	50	10	0.81	1714	934	10.8	122.7	365		
T20	more fuel	125	2.66	2.27 x10 ⁻³								1.00	1894	1034	10.95	124.4	157		
T21	fuel @ 30F	105	2.46	2.10 x10 ⁻³	30	-1	42	6	50	10	0.92	1932	1056	9.34	106.1	211			
T22	fuel @ 70F				70	21					0.92	1916	1047	8.4	95.4	189			
T23	fuel @ 90F				90	32					0.92	1870	1021	9.91	112.5	209			
T24	less air				45	239					3.01 x10 ⁻²	0.89	1924	1051	9.69	110	128		
T25	more air	58	293	3.69 x10 ⁻²	42	6	50	265	3.34 x10 ⁻²	50	10	0.9	1932	1056	9.49	107.8	270		
T26	air @ 40 F	50	265	3.34 x10 ⁻²								40	4	0.92	1945	1063	10.06	114.2	211
T27	air @ 80 F	52										80	27	0.92	1953	1067	11.63	132.1	185
T28	air @ 100 F	53										100	38	0.92	1878	1026	10.25	116.4	191

B-4

Table B-7. Detailed test conditions for impact of burner configuration (updated configuration)

Test Case	Description	Fuel					Air					Φ	Avg T		Heat Flux		BT
		psi	GPH	kg/s	°F	°C	psig	pph	kg/s	°F	°C		°F	°C	BTU/ft ² -s	kW/m ²	sec
T29	Baseline	109	2.5	2.13x 10 ⁻³	42	6	50	265	3.34x 10 ⁻²	50	10	0.9 4	1900	1038	10.2	115.8	190
T30													1910	1043	11.1	126.1	184
T31													1855	1013	11	124.9	163
T32													1875	1024	11.9	135.1	183
T33													1855	1013	11.5	130.6	163
T34													1866	1019	11.7	132.9	160
T35	Nozzle @ -12.7												1880	1027	10	113.6	170
T36													1870	1021	8.2	93.1	182
T37	Nozzle @ +12.7												1900	1038	10.5	119.2	206
T38													1885	1029	10.9	123.8	206
T39	Cone @ -50.8												1896	1036	11.4	129.5	162
T40	Cone @ -25.4												1908	1042	10.7	121.5	180
T41	Cone @ +25.4												1920	1049	8.5	96.5	206
T42	Cone @ +50.8												1850	1010	10.2	115.8	221
T43	Ceramic insulated cone												1917	1047	10.7	121.5	162
T44													1935	1057	11.6	131.7	163
T45	Inconel cone												1890	1032	11.1	126.1	143
T46													1854	1012	11.4	129.5	136
T47	FAA cone design												1890	1032	8.2	93.1	165
T48													1888	1031	10.1	114.7	152
T49	Slightly deformed FRH	1720	938	10.9	123.8	170											
T50		1815	991	11.2	127.2	172											
T51	Severely deformed FRH	1841	1005	10.2	115.8	154											
T52		1795	979	9.4	106.8	181											

B-5